Dynamic Micropatterning Reveals Substrate-Dependent Differences in the Geometric Control of Cell Polarization and Migration

Isomursu, Aleksi; Alanko, Jonna; Hernández-Pérez, Sara; Saukkonen, Karla; Saari, Markku; Mattila, Pieta K.; Ivaska, Johanna

Published in:
Small Methods

DOI:
10.1002/smtd.202300719

Published: 01/01/2024

Document Version
Final published version

Document License
CC BY

small methods
www.small-methods.com

Dynamic Micropatterning Reveals Substrate-Dependent Differences in the Geometric Control of Cell Polarization and Migration

*Aleksi Isomursu, Jonna Alanko, Sara Hernández-Pérez, Karla Saukkonen, Markku Saari, Pieta K. Mattila, and Johanna Ivaska**

Cells are highly dynamic and adopt variable shapes and sizes. These variations are biologically important but challenging to investigate in a spatiotemporally controlled manner. Micropatterning, confining cells on microfabricated substrates with defined geometries and molecular compositions, is a powerful tool for controlling cell shape and interactions. However, conventional binary micropatterns are static and fail to address dynamic changes in cell polarity, spreading, and migration. Here, a method for dynamic micropatterning is reported, where the non-adhesive surface surrounding adhesive micropatterns is rapidly converted to support specific cell-matrix interactions while allowing simultaneous imaging of the cells. The technique is based on ultraviolet photopatterning of biotinylated polyethylene glycol-grafted poly-L-lysine, and it is simple, inexpensive, and compatible with a wide range of streptavidin-conjugated ligands. Experiments using biotinylation-based dynamic micropatterns reveal that distinct extracellular matrix ligands and bivalent integrin-clustering antibodies support different degrees of front-rear polarity in human glioblastoma cells, which correlates to altered directionality and persistence upon release and migration on fibronectin. Unexpectedly, however, neither an asymmetric cell shape nor centrosome orientation can fully predict the future direction of migration. Taken together, biotinylation-based dynamic micropatterns allow easily accessible and highly customizable control over cell morphology and motility.

1. Introduction

A major challenge in investigating biological processes is the inherent variability present in all living systems, from single cells to complex multicellular organisms. Micropatterning, i.e., confining cells spatially on substrates of predefined shape, size, and molecular composition, is a powerful tool for standardizing the intracellular organization of individual cells for research purposes.[1–3] In addition, micropatterning can be used for investigating the impact of different cell–cell and cell-extracellular matrix (ECM) interactions on cell fate and function, allowing reproducible modeling of different niche architectures.[4–7] Typically, the cell adhesion-permissive surfaces of conventional binary micropatterns are surrounded by inert, permanently non-adhesive regions. While useful, such static micropatterns are ill-suited for investigating dynamic cellular processes, including cell spreading and migration. To circumvent this limitation, different

A. Isomursu, J. Alanko, S. Hernández-Pérez, K. Saukkonen, M. Saari, P. K. Mattila, J. Ivaska
Turku Bioscience Centre
University of Turku and Åbo Akademi University
Turku 20520, Finland
E-mail: johanna.ivaska@utu.fi

S. Hernández-Pérez, P. K. Mattila
Institute of Biomedicine and MediCity Research Laboratories
University of Turku
Turku 20014, Finland

S. Hernández-Pérez, P. K. Mattila, J. Ivaska
Department of Life Technologies
University of Turku
Turku 20520, Finland

J. Ivaska
InFLAMES Research Flagship Center
University of Turku
Turku 20520, Finland

J. Ivaska
Western Finnish Cancer Center (FICAN West)
University of Turku
Turku 20520, Finland

J. Ivaska
Foundation for the Finnish Cancer Institute
Helsinki 00014, Finland

The ORCID identification number(s) for the author(s) of this article can be found under https://doi.org/10.1002/smtd.202300719

DOI: 10.1002/smtd.202300719

techniques for reversible, or dynamic, micropatterning have been developed.

In dynamic micropatterning, specific substrate regions can be made permissive (or non-permissive) for cell adhesion at will. Cell-repellent surface treatments can be removed or bioactive ligand molecules uncaged using light,[8–12] electric voltage,[13–16] or changes in temperature.[17,18] However, many of these methods rely on non-specific adsorption of ECM components or other ligand molecules from the growth medium, limiting the amount of control the user has over specific cell-ECM interactions. While the physical stimuli used for substrate modifications are generally well tolerated by cells, significant changes in temperature, electric potential differences, or high-energy light may all affect particularly sensitive biological systems, impacting the interpretation of the results.[19,20] Many controlled desorption methods also require specialized equipment or techniques, such as microfabricated electrodes or synthesis of heat- or electrosensitive surface coatings, which can limit their adoption by the wider research community. Such specialized methods include also the maskless photopatterning[21] system PRIMO (Alvéole). Blue light and a separate photoinitiator (4-benzoylbenzyl-trimethylammonium chloride) allow highly versatile patterning of different ligand molecule combinations on polyethylene glycol-grafted poly-L-lysine (PLL-g-PEG) surfaces. However, the system's reliance on reactive species derived from the photoinitiator can limit its use for dynamic micropatterning with live cells. In addition, acquiring the system represents a significant financial investment for an individual research group or facility.

Cell attachment to previously non-adhesive regions can also be achieved via selective addition of specific secondary ligands. Sequential microcontact printing of ECM components and neutravidin allows a controlled release of cells from micropatterns on biotinylated ECM molecules.[22] The method benefits from high spatial resolution and the significant strength of its biotin-avidin capture chemistry, however, it is also subject to the usual technical challenges of microcontact printing: for example, low stamp aspect ratios can result in a roof collapse, restricting the available pattern geometries and spacing.[23] Alternatively, dynamic micropatterns can be engineered using so-called click chemistries, fast and high-yielding conjugations of molecular entities. Examples of these include 1) light-activated thiol-ene/yne coupling of Arg-Gly-Asp (RGD)-containing synthetic peptides to polyethylene glycol methacrylate-stamped coverslips[24,25] and 2) strain-promoted azide-alkyne cycloaddition of another modified RGD-peptide, bicyclononyne-RGD, to photopatterned azido-PLL-g-PEG surfaces.[26] While fast and efficient, both methods necessitate extensive synthesis and/or use of specific custom peptides, which significantly restricts the amount of compatible secondary ligands.

One field of biological research that has benefited from the use of micropatterning is the study of planar polarity in directed cell migration.[15,27–30] Most cells in the human body are polarized, showing some degree of shape and functional asymmetry that is critical for normal homeostasis. Migratory cells organize their adhesive and cytoskeletal machinery and intracellular organelles in a front-rear polarized manner, where effective polarization depends on careful spatiotemporal regulation of different polarity factors, especially the small GTPases of the Rho family.[31,32] Gradients of Cdc42, Rac, Rho and their respective upstream regulators like β-PIX can arise stochastically or as a response to different extracellular cues. Downstream of the Rho GTPases, additional polarity factors like the Par6/aPKC complex and its targets help regulate cytoskeletal dynamics, driving protrusion and contractility, and organize the rest of the intracellular machinery to support persistent migration.[33–35] In particular, the Golgi apparatus and centrosome, both of which can function as microtubule-organizing centers (MTOC), are aligned relative to the other organelles and the leading edge of the cell.[1,36–39] In mesenchymal cells migrating in 2D environments, the MTOC almost invariably resides in front of the nucleus and faces the leading edge of the cell. This organizes and orients the microtubule array toward the leading edge, which helps tune adhesion dynamics and supports anterograde trafficking of polarity factors, leading to persistent protrusion and migration.[38,40–45]

Front-rear polarity and cell migration have often been investigated using the so-called scratch-wound assay,[38,42,46,47] where cells in a monolayer polarize and migrate toward an unoccupied adhesive region. While this approach has uncovered many key mechanisms of directed cell migration, it is limited to exploration of cell behavior on uniform ECM. Human tissues, on the other hand, are composed of complex mixtures of ECM components and cells engage these using different subsets of integrin cell adhesion receptors.[48] Indeed, integrin adhesion complexes are key upstream regulators of cell front-rear polarity and directed migration, including polarization in response to substrate geometry.[1,30,49,50] ECM composition is also known to impact the organization of epithelia, including their apicobasal polarity,[51,52] and fibronectin concentration has been suggested to influence the front-rear polarization of CHO cells.[50] In addition, Rho GTPases have been shown to impact 3D migration differently in collagen- and fibronectin-rich environments, with β-PIX being recruited to the leading edge of human foreskin fibroblasts to regulate Cdc42 activation only in collagen matrices.[53] However, systematic studies on planar polarity and directed migration in response to altered ECM landscapes have not been conducted.

To facilitate investigation of the influence of ECM composition on cell polarity and migration, we developed a new, readily accessible, and inexpensive method for dynamic micropatterning. The method is based on ultraviolet (UV) photopatterning[54] of biotinylated PLL-g-PEG. By using streptavidin-conjugated secondary ligands, such as different ECM proteins or antibodies, the new technique enables versatile micropatterning with different adaptations: 1) conventional binary micropatterning of adhesive and non-adhesive regions, 2) generating dual micropatterns with alternating regions of two mutually exclusive ligands of interest, and 3) reversible micropatterning, where the cells adhering to a specific ligand can be rapidly released from their spatial confinement to adhere and spread onto a new ligand. We demonstrated the adaptability of the technique by studying cell adhesion and polarization using different cancer cell lines, and the formation of the immune synapse in B lymphocytes (B cells). In particular, we investigated the impact of ECM composition on the front-rear polarity and directed migration of human cancer cells, and found that integrin binding to different ECM ligands or bivalent integrin-clustering antibodies can support different degrees of centrosome orientation toward the leading edge of the cell. On anisotropic micropatterns, fibronectin and laminin-521

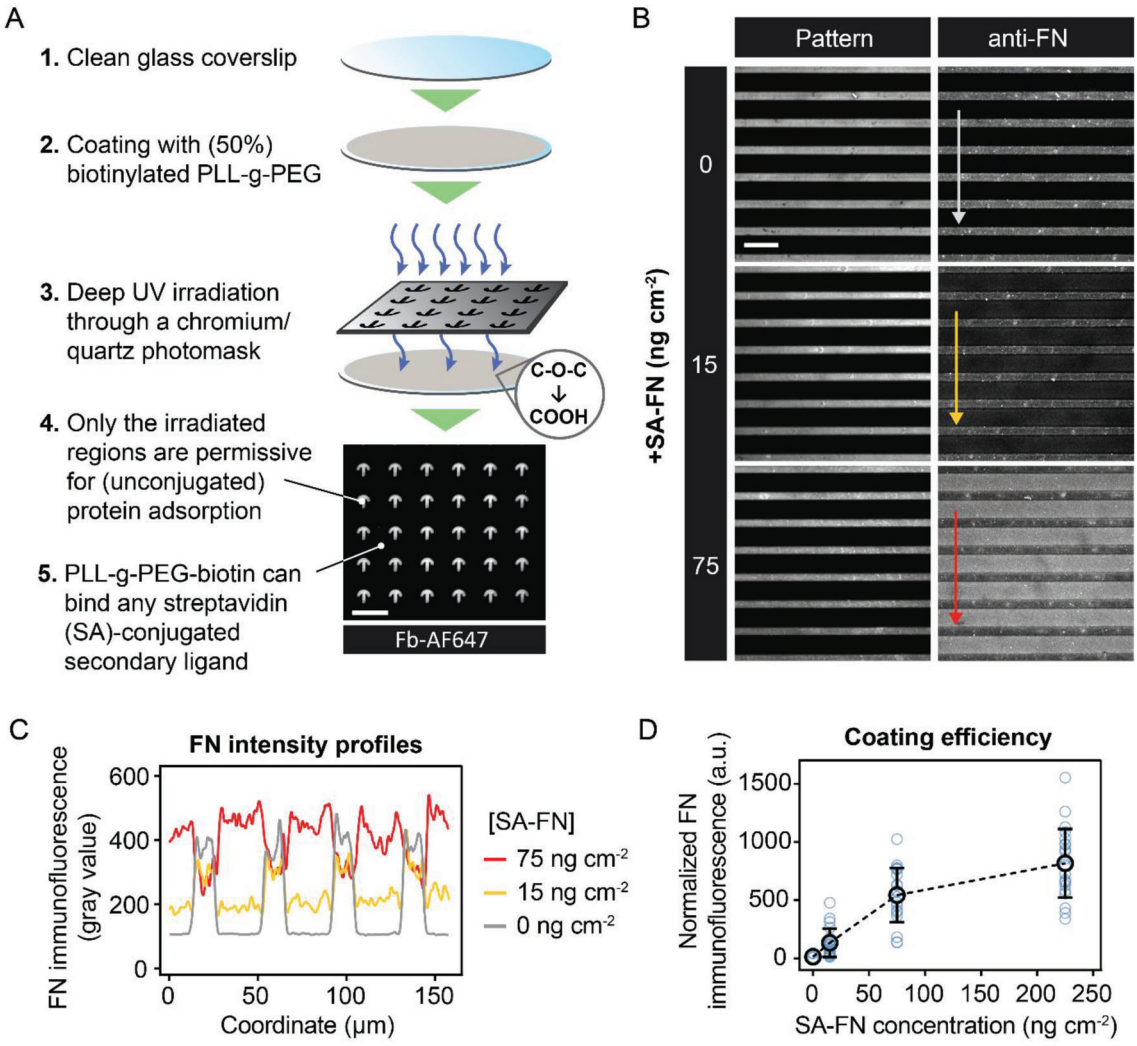

(LN-521) coating were the strongest inducers of planar polarity, while type I collagen and different integrin β1-binding antibodies could elicit only partial polarization. The higher front-rear polarity on fibronectin-coated micropatterns correlated with more polarized and directionally persistent migration when the cells were released on fibronectin. However, at the level of individual cells, initial centrosome orientation poorly predicted the future direction of migration.

2. Results and Discussion

In order to overcome many of the limitations of the existing micropatterning methods, we started by coating acid-washed and ultraviolet ozone (UVO)-cleaned glass coverslips with 50% biotinylated PLL-g-PEG. The resulting coverslips were photopatterned using deep UV light to yield planar substrates with protein adsorption permissive (carboxyl group-containing) and nonpermissive regions (**Figure 1**A; Figure S1A, Supporting Information).[54] In order to coat the photopatterned regions with proteins, the coverslips were incubated in a mixture of fibronectin and fluorescently labeled bovine serum albumin (BSA), an inert protein included at low concentrations to aid visualization of the micropatterns. Next, by incubating the coverslips with different concentrations of streptavidin-conjugated fibronectin (SA-FN) and visualizing the resulting substrates by immunofluorescence microscopy, we observed a gradual increase in the amount of bound fibronectin in the regions surrounding the micropatterns. In comparison, the amount of fibronectin on the micropatterns themselves was not markedly affected by the addition of the secondary ligand (Figure 1B,C). The fibronectin content of substrate regions outside the micropatterns increased linearly as a function of exogenous SA-FN before starting to plateau, likely due to saturation of the biotinylated PLL-g-PEG (Figure 1D).

The bond between streptavidin and biotin is exceptionally strong ($K_d \approx 10^{-14}$ M),[55] and consequently any PLL-g-PEG-biotin surfaces coated with streptavidin-conjugated secondary ligands are expected to be very stable in normal cell culture conditions. To test this, we prepared coverslips with biotinylated PLL-g-PEG, coated them with SA-FN, and incubated them in a normal growth medium, at +37 °C in a humidified incubator, for 1 to 6 days. We did not observe any decrease in surface fibronectin density over time (Figure S1B,C, Supporting Information). Furthermore, the SA-FN surfaces remained fully amenable for cell culture over the course of the experiment, supporting the adhesion and growth of U-251MG glioblastoma cells for up to 6 days (Figure S1D, Supporting Information).

In order to further confirm the specificity of protein coating in both photopatterned and nonpatterned substrate regions, we prepared additional coverslips with thin linear micropatterns that: 1) were coated with an adhesive ECM component and integrin ligand, collagen, and no secondary ligand, or 2) were first blocked using (fluorescent) BSA and the surrounding substrate was subsequently coated with streptavidin-conjugated collagen-mimetic peptide, SA-GFOGER. Next, the substrates were seeded with MDA-MB-231 breast adenocarcinoma cells that were allowed to spread for 3 h before the samples were fixed, and integrin-mediated cell-ECM adhesions were visualized by paxillin immunofluorescence. On both substrates, paxillin-positive adhesions were confined to substrate regions coated with integrin ligands, whether on the actual micropatterns or surrounding them (Figure 1E). Taken together, these data indicate that UV photopatterning of PLL-g-PEG-biotin can be combined with streptavidin-conjugated secondary ligands to rapidly and easily yield binary micropatterns with two mutually exclusive coating modalities.

Next, we wanted to confirm that PLL-g-PEG biotinylation does not interfere with normal cell morphology and function on the micropatterned substrates. To this end, we seeded U-251MG cells and U-2OS osteosarcoma cells on crossbow-shaped, fibronectin-coated micropatterns prepared on unmodified and 50% biotinylated PLL-g-PEG. There were no obvious differences in the actin cytoskeleton or integrin-mediated adhesions (visualized by paxillin staining) between the cells on either substrate but, as expected, the U-2OS cells presented with larger focal adhesions and more prominent ventral stress fibers than the glioma cells (**Figure 2**A,B; Figure S2A,B, Supporting Information).[56,57]

One of the most interesting implications of replacing unmodified PLL-g-PEG with biotinylated compound is the possibility of using streptavidin-conjugated secondary ligands for dynamic micropatterning in live-cell experiments (Figure 2C). We tested this possibility by growing U-2OS cells on fibronectin-coated micropatterns and supplementing selected cultures with streptavidin-conjugated fibronectin fragment, SA-FNIII 7–10, 1 h before the samples were fixed and processed for immunofluorescence microscopy. As expected, cells grown on micropatterned PLL-g-PEG-biotin and supplemented with SA-FNIII 7–10 had rapidly spread on the surrounding substrate, while the cells on unmodified PLL-g-PEG remained strictly confined to the crossbow-shaped micropatterns, despite the addition of the secondary ligand (Figure 2D).

The rapid release of U-2OS cells from the micropatterns and the strength of the biotin-streptavidin interaction both suggested

Figure 1. Binary micropatterning using biotinylated PLL-g-PEG and streptavidin-conjugated secondary ligands. A) Schematic representation of the technique. Combining biotinylated antifouling agent PLL-g-PEG with deep UV photopatterning allows the preparation of glass coverslips with defined regions coated with two different molecules of interest. Scale bar, 100 µm. Fb, fibrinogen. B,C) Fluorescence images (B) and intensity profiles (C) depicting micropatterned coverslips (225 ng cm^{-2} FN + 75 ng cm^{-2} BSA-AF555) incubated with varying concentrations of streptavidin-conjugated secondary ligand (SA-FN). The FN density outside photopatterned regions, visualized by immunofluorescence, is scalable and can be higher than the amount of protein adsorbed to the original patterns. Representative of two independent experiments. D) Quantified immunofluorescence data displaying the concentration of SA-FN on micropatterned PLL-g-PEG-biotin coverslips, outside the micropatterns, as a function of total SA-FN added. Mean ± SD of n = 18 (0 ng cm^{-2}), 26 (15 ng cm^{-2}), 20 (75 ng cm^{-2}), and 22 (225 ng cm^{-2}) fields of view. Data normalized to the area under the curve and pooled from three independent experiments. E) Fluorescence images of MDA-MB-231 cells on micropatterned coverslips coated with two different combinations of primary and secondary ligands. Either the patterns have been coated with integrin ligand (225 ng cm^{-2} collagen + 75 ng cm^{-2} BSA-AF555) (top), or they have been visualized with labeled BSA and the surrounding area has been coated with SA-conjugated GFOGER peptide (75 ng cm^{-2}) to make it permissive for cell adhesion (bottom). All images represent individual focal planes. Scale bars, 10 µm (main) and 5 µm (ROI). Representative of two independent experiments.

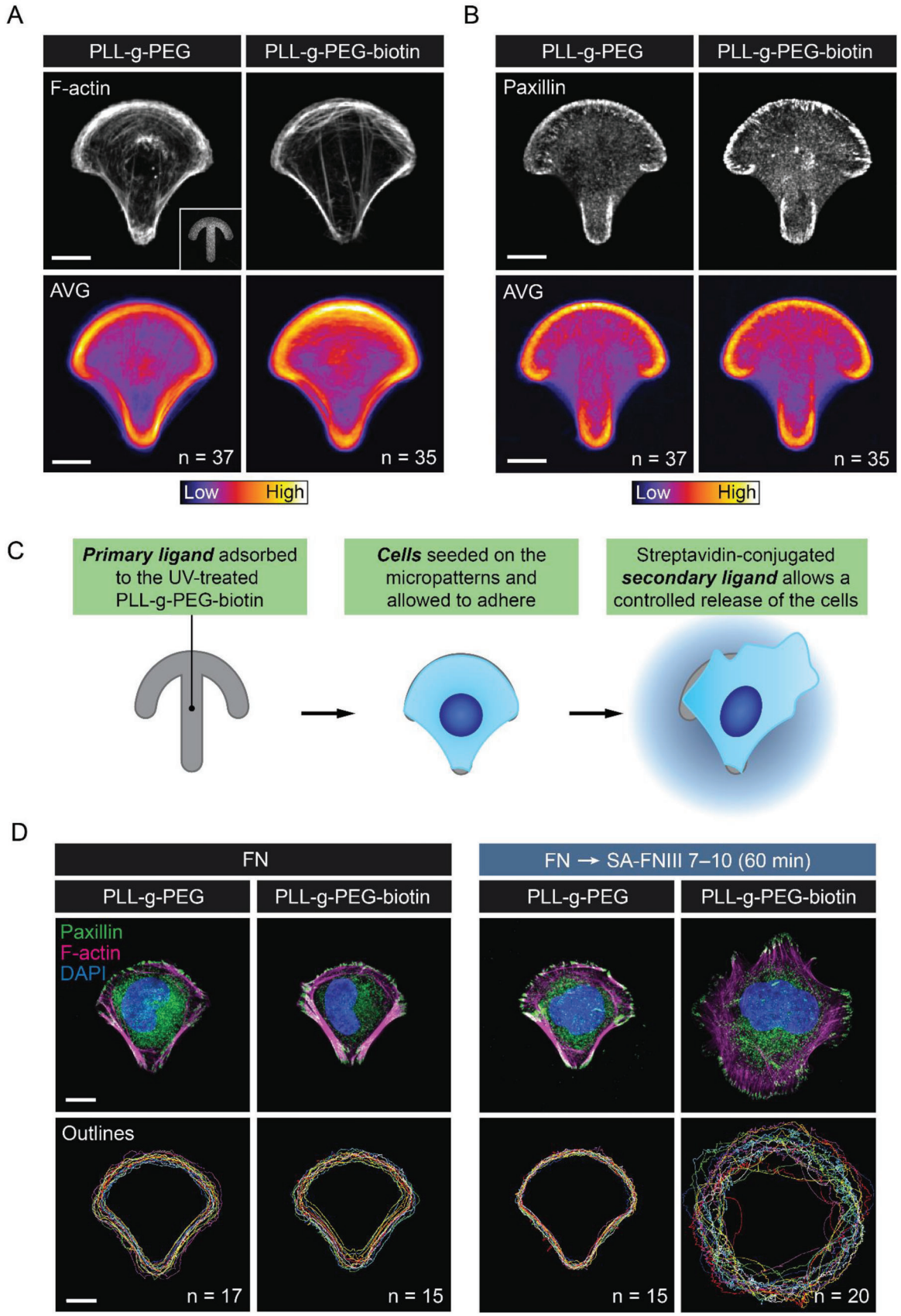

that the process of coating the free PLL-g-PEG-biotin with SA-FN would occur very quickly. To investigate this, we used fibronectin conjugated to both streptavidin and fluorescein isothiocyanate (SA-FN-FITC). Confocal microscopy movies of micropatterned PLL-g-PEG-biotin coverslips revealed that the binding of SA-FN-FITC to the non-UV-irradiated coverslip surface was almost instantaneous (<2 min), with most of the remaining secondary ligand diffusing across the imaging chamber and disappearing from the growth medium in ≈ 15 min (Figure S1E–G; Video S1, Supporting Information).

To further validate the technique using a different cell type and ligand, we decided to test its applicability for controlling B cell activation. B cells respond to antigens by forming an intricate cell-cell (or cell-matrix) interaction structure known as the immune synapse.[58] A20 mouse lymphoma cells expressing IgM B cell antigen receptor (BCR) can be activated using anti-IgM antibodies as surrogate antigens, however, monovalent Fab fragments of the surrogate antigen are unable to trigger the BCR unless they are tethered to a surface.[59,60] By using streptavidin-coupled anti-IgM Fab (SA-anti-IgM Fab), B cell activation can be directed exclusively to the biotinylated substrate, which allows in vitro modeling of immune synapse formation from the very beginning of BCR engagement.

We prepared small ($\varnothing = 5$ µm) round micropatterns on PLL-g-PEG-biotin, coated them with fibronectin, and seeded the substrates with A20 cells. Fibronectin allows B cell adhesion, but it does not support their activation. We then supplemented the micropatterned A20 cells with unconjugated or SA-anti-IgM Fab and incubated them for 10 min. The cells supplemented with SA-anti-IgM Fab spread rapidly outward from the original micropatterns, displaying radial symmetric actin architectures characteristic of developing immune synapses (Figure S3A–C, Supporting Information).[58,61] In contrast, the cells supplemented with unconjugated Fab remained spherical and fully confined to the adhesive micropatterns. Together, the above results clearly illustrate that photopatterned PLL-g-PEG-biotin and streptavidin-conjugated secondary ligands can be used for dynamic micropatterning of different adhesive substrates. The release of micropatterned cells from their confinement is rapid and requires the presence of both biotin and streptavidin groups. This is an important consideration for many experiments since the strength of the streptavidin-biotin interaction helps prevent possible ligand delamination from the otherwise weakly adsorptive PEG, improving the interpretation of the data.[62,63]

Many factors are known to influence planar polarity, but systematic comparisons of cell adhesion to different integrin ligands/ECM components have been lacking. Therefore, we investigated whether front-rear polarization by geometric cues can be influenced by the type of ECM the cells are interacting with. We started by growing U-251MG cells on crossbow-shaped micropatterns coated with different substrate molecules. These included fibronectin and type I collagen, fibrillar ECM components common to many tissues and often enriched in solid tumors, and LN-521, a basement membrane (BM) component considered ubiquitous to most human BMs and widely recognized by different integrin β1-containing heterodimers.[64,65] All substrate comparisons were conducted after blocking the coated micropatterns with 2% BSA, and fibronectin-depleted serum was used to supplement the growth media (Figure S4A, Supporting Information). Front-rear polarization was evaluated based on the orientation of the perinuclear centrosome, indicated by γ-tubulin or centrin-2, relative to the nucleus. We also observed a previously reported[47] colocalization of paxillin with the centrosome (**Figure 3**A). As expected, U-251MG cells were highly polarized on the fibronectin-coated micropatterns, their centrosomes residing mainly between their nuclei and the wide, adhesive edges of the crossbow-shaped patterns (Figure 3A,B; Figure S4B, Supporting Information). The same was true for cells on LN-521. In contrast, cells grown on collagen-coated patterns were significantly less polarized than their fibronectin-adhered counterparts (Figure 3A,B; Figure S4B, Supporting Information). Similar results were obtained when using the orientation of the trans-Golgi network as a proxy for front-rear polarization (Figure S4C,D, Supporting Information).

We wanted to investigate whether these differences could result from a reduced ability of the U-251MG cells to generate integrin-mediated adhesions on type I collagen. First, we noted that the cells could spread on collagen-coated micropatterns as quickly and efficiently as on fibronectin, whereas the number and size of integrin-mediated adhesions, indicated by paxillin staining, varied considerably between individual cells. We then compared the average distribution of paxillin-positive adhesions in micropatterned U-251MG cells on each of the different ECM components (Figure S5, Supporting Information). While the mean paxillin density in peripheral lamellipodia or the cell rear did not differ markedly between collagen and fibronectin or LN-521, we did observe more diffuse paxillin signal throughout the basal sides of collagen-adhered cells. The relative variation in peripheral paxillin density was also slightly higher on collagen. This indicates that the overall spatial distribution of adhesions in U-251MG cells is less tightly regulated on collagen, which may contribute to the more inconsistent polarization on collagen-coated micropatterns.

Integrin ligation to a substrate and integrin clustering on the plasma membrane are known to elicit distinct but partially overlapping signaling responses in cells.[66,67] To further explore the dependency of polarization on integrin signaling, and to decouple these two cues, we generated micropatterns coated with

Figure 2. PLL-g-PEG biotinylation does not interfere with normal cell morphology but allows a controlled release of cells from the micropatterns. A) Fluorescence images (top) and average intensity projections (bottom) of n = 35–37 U-251MG cells depicting actin organization in cells plated on crossbow-shaped, FN-coated micropatterns (inset, visualized by Fb-AF647) on either non- or 50% biotinylated PLL-g-PEG. Scale bars, 10 µm. Representative of three independent experiments. B) As in (A), but instead of actin, paxillin has been visualized by immunofluorescence. C) Schematic representation of biotinylation-based dynamic micropatterning. After cells have adhered to the micropatterns, the remaining substrate surface can be made permissive for cell attachment by adding a streptavidin-conjugated secondary ligand. D) Immunofluorescence images (top) and overlaid cell outlines (bottom) depicting n = 15–20 U-2OS cells on crossbow-shaped, FN-coated micropatterns after 4 h of spreading, without (left) or with (right) 150 ng cm^{-2} of SA-FNIII 7–10 added in the medium for the last 60 min. The patterns were prepared on non- or 50% biotinylated PLL-g-PEG as indicated. Scale bar, 10 µm. Representative of three independent experiments.

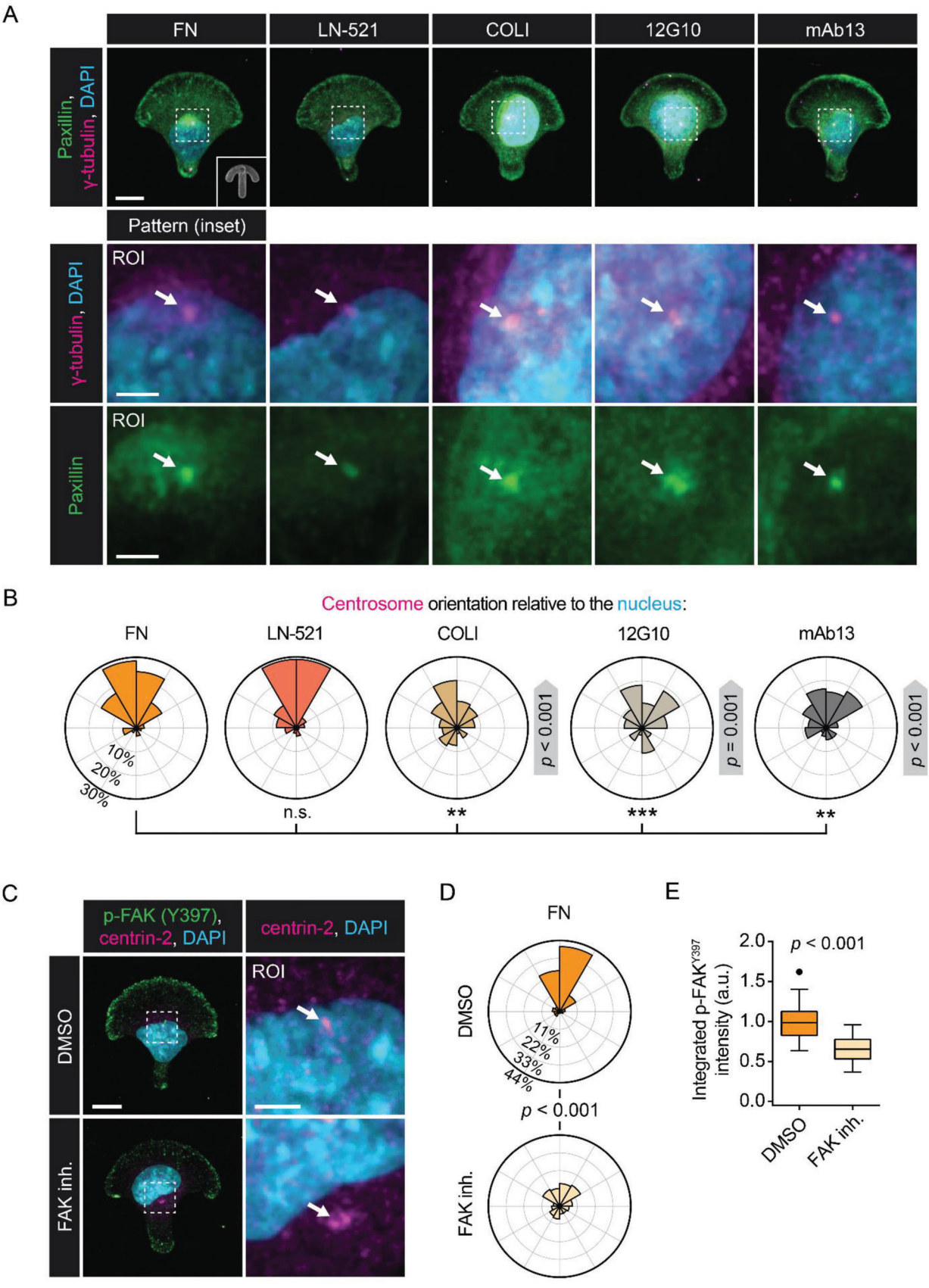

bivalent antibodies raised against the active (extended-open; clone 12G10) or inactive (bent-closed; clone mAb13) conformations of integrin β1. Interestingly, both integrin β1-targeting antibodies were capable of supporting at least partial front-rear polarization on anisotropic micropatterns: while the overall distribution of organelles in individual cells was less uniform than on fibronectin or LN-521 and resembled the collagen-adhered cells, there was still a significant tendency for the centrosomes to face the wide adhesive edge of the micropattern (Figure 3A,B; Figure S4B, Supporting Information).

Intrigued by this observation, we sought to investigate the differences in integrin-mediated signaling elicited by the different substrates. We seeded U-251MG cells on polystyrene plates coated with fibronectin, collagen, 12G10, or mAb13, lyzed the cells after 30 min, and used western blotting to compare their signaling responses to cells that had been kept suspended in growth medium (i.e., negative control) (Figure S6A–C, Supporting Information). Surprisingly, we observed almost no differences in protein kinase B (AKT) phosphorylation (S473), and extracellular signal-regulated kinase 1/2 (ERK1/2) phosphorylation (T202/Y204) was barely affected by any of the substrates excluding the negative control, wherein the amount of phospho-ERK was markedly lower (Figure S6B,C, Supporting Information). However, the phosphorylation (Y397) of focal adhesion kinase (FAK) exhibited a downward trend from fibronectin to collagen to 12G10 and mAb13 (Figure S6B,C, Supporting Information). Since FAK activation has been previously deemed important for planar polarity in migrating cells,[46,47,68] we treated U-251MG cells on fibronectin-coated crossbow-shaped micropatterns with a FAK inhibitor, PF-573228, and observed a significant decrease in both front-rear polarization and the amount of phospho-FAK present in the cells (Figure 3C–E). Taken together, these results indicate that the choice of biological substrate can significantly impact the capacity of cells to polarize in response to geometric cues, and FAK activity is needed to maintain the maximal front-rear polarity of U-251MG cells on fibronectin. However, even integrin-clustering anti-integrin β1 antibodies can induce significant signaling responses and support partial polarization of cells in anisotropic environments, irrespective of the associated integrin conformation.

Since anisotropic micropatterns have been used for both studying and directing cell motility, and centrosome orientation has been considered a key polarization step preceding directed migration, we wanted to use biotinylation-based dynamic micropatterning to investigate the impact different substrates can have on directed cell spreading and migration. We seeded stably EGFP-centrin-2-expressing U-251MG cells on crossbow-shaped micropatterns coated with fibronectin or mAb13. After the cells had adhered and occupied the pattern area, they were supplemented with SA-FN to release them from their confinement, and tracked over time (**Figure 4**A; Figure S7A and Video S2, Supporting Information). On average, the cells spread rapidly from both substrates, reaching their final size and sometimes leaving the micropattern entirely in only 60 min (Figure 4B,C). Centrosome orientation just prior to the addition of SA-FN was consistent with the experiments in, e.g., Figure 3A,B, with mAb13-adhered cells displaying decreased front-rear polarity (Figure 4D). The early spreading and migration of cells leaving the mAb13-coated patterns also appeared less polarized, consistent with the idea of centrosome orientation regulating cell protrusion and migration (Figure 4E).

To further elucidate these differences, we continued tracking the cells for 4 h after the addition of SA-FN (Figure S7B, Supporting Information). Indeed, cells released from fibronectin-coated micropatterns migrated with higher directional persistence, but this did not coincide with longer tracks; if anything, the cells leaving mAb13 patterns migrated faster but with less persistence (Figure S7C–E, Supporting Information). This latter observation could possibly be attributed to the fact that the mAb13-coated micropattern itself is not the preferred substrate for the cells, and any cells released from these patterns are more prone to rapidly generating new adhesions and spreading when the physiological ligand, fibronectin, is provided.

Another aspect of the cytoskeletal and adhesive machinery that has been linked to cell polarity is actin retrograde flow. Plasma membrane tension and forces exerted by molecular motors push and pull filamentous actin away from the leading edge and toward the perinuclear region. At the same time, this motion is resisted by cell adhesion molecules, typically integrins and their various adaptors, that link the intracellular cytoskeleton to the ECM to drive cell migration.[69–71] Actin flow may promote front-rear polarization by redistributing specific polarity factors and cytoskeletal regulators inside the cell, or more directly, by moving the nucleus backward and behind the MTOC.[33,72] As integrins play a key role in resisting the actin retrograde flow, confining cells spatially on micropatterns is expected to promote actin flow by preventing protrusion and adhesion in front of the pre-existing leading edge. To investigate whether actin dynamics on anisotropic micropatterns are affected by the choice of substrate (fibronectin vs. mAb13), we first recorded actin retrograde flow in U-251MG cells plated on micropatterns. We did not observe any significant differences in actin retrograde flow between the

Figure 3. Different integrin ligands and FAK activity both influence front-rear polarization and organelle rearrangement on anisotropic micropatterns. A) Immunofluorescence images of U-251MG cells on crossbow-shaped micropatterns coated with different ECM components or integrin β1-targeting monoclonal antibodies (750 ng cm^{-2}). The micropatterns were visualized by BSA-AF555 (inset, 75 ng cm^{-2}). ROIs depict centrosomes (white arrows), visualized by staining of γ-tubulin and paxillin. Scale bars, 10 µm (main) and 3 µm (ROI). Representative of two independent experiments. B) Angular histograms depicting centrosome orientation relative to the nucleus in the cells in (A). The wide adhesive edge of the micropattern is aligned toward the top. Values from $n = 89$ (FN), 82 (LN-521), 81 (COLI), 67 (12G10), and 80 (mAb13) cells, from two independent experiments. N.s. $p > 0.05$, $^{**}p < 0.01$, $^{***}p < 0.001$. Analyzed by Watson's U2 test (pairwise comparisons) and Rayleigh test (non-uniformity, gray arrows). C) Immunofluorescence images depicting phosphorylated FAK and centrosomes (centrin-2, white arrows) in U-251MG cells plated on crossbow-shaped, FN-coated micropatterns and treated with FAK inhibitor PF-573228 (5 µM for 90 min) or vehicle. Phospho-FAK represents a single focal plane from the basal side of the cell, while the other channels are maximum-intensity projections. Scale bars, 10 µm (main) and 3 µm (ROI). Representative of three independent experiments. D) Angular histograms depicting centrosome orientation relative to the nucleus in the cells in (C). $n = 88$ (DMSO)–101 (FAK inh.) cells from three independent experiments. Analyzed by Watson's U2 test. E) Integrated basal phospho-FAK immunofluorescence in the cells in (C). $n = 27$ (DMSO)–31 (FAK inh.) cells from a representative of three independent experiments. Analyzed by Welch's t-test.

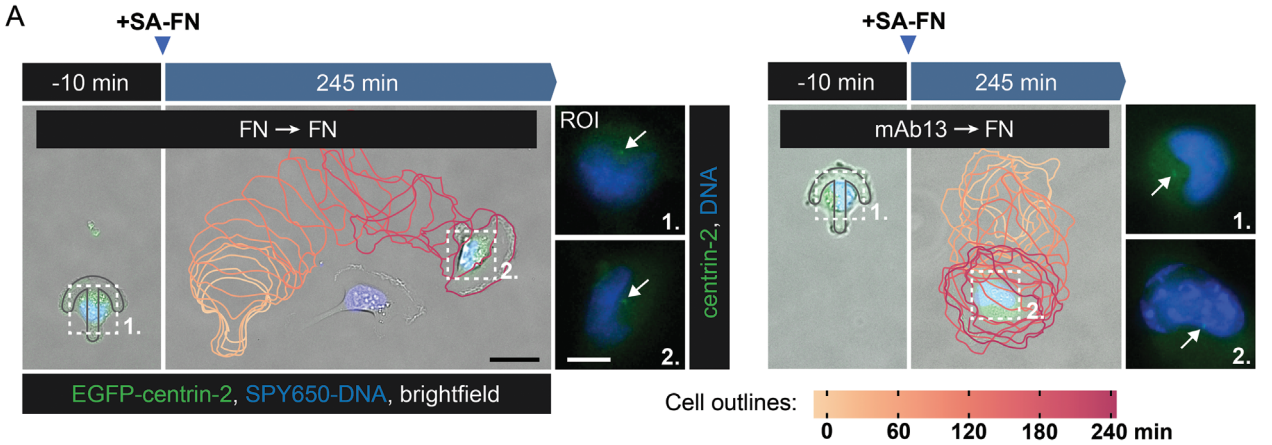

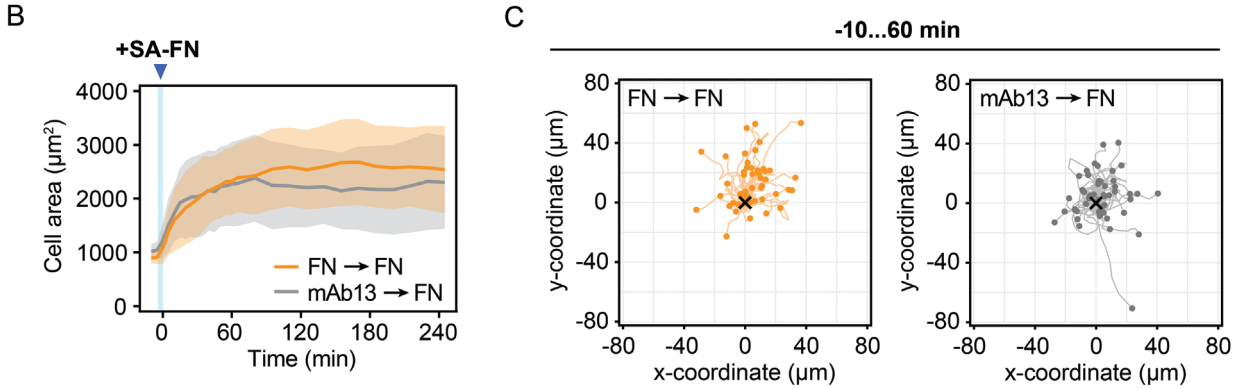

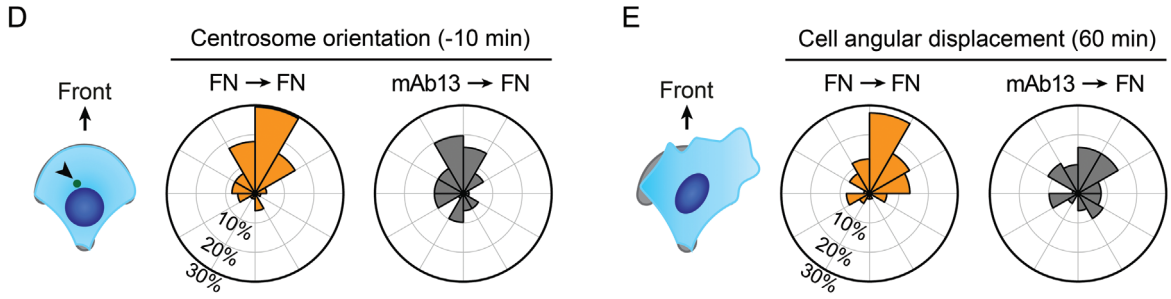

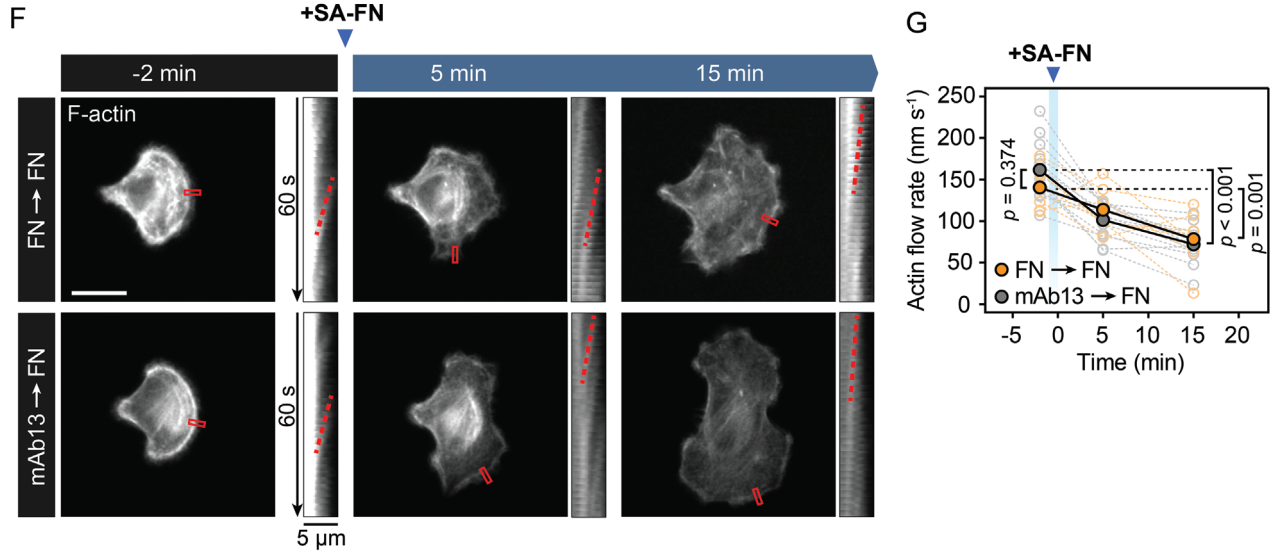

cells on fibronectin- and mAb13-coated micropatterns, implying that differences in actin flow dynamics are not a major contributing factor behind the lower front-rear polarity of mAb13-adhered cells (Figure 4F,G). Next, we explored the outcome of secondary ligand-mediated cell spreading on actin dynamics by releasing the cells from fibronectin or mAb13 on SA-FN. As expected, releasing the cells led to a rapid decrease in the actin flow rate, irrespective of the original substrate (Figure 4F,G; Video S3, Supporting Information). These data show that dynamic micropatterning is a valuable method for investigating actin dynamics upon spatially and temporally controlled alterations to cell shape. Furthermore, our data demonstrate that actin dynamics are strongly linked to the ability of cells to spread and protrude but, at least under the conditions reported here, the nature of the integrin-engaging substrate is less critical.

We were intrigued by the finding that plating cells on mAb13-coated micropatterns lowered the cells' front-rear polarity and tendency to migrate forward upon release. To further explore this, we analyzed the extent to which centrosome orientation correlates with the direction of U-251MG migration. We stratified the cells in Figure 4C into two groups based on their initial centrosome orientation: one group for cells with centrosomes in front of their nuclei (i.e., facing the wide adhesive edge of the micropattern), and one for those with centrosomes in the back. To our surprise, we found that the initial centrosome orientation only poorly predicted the direction of migration upon subsequent addition of SA-FN (**Figure 5**A,B; Video S4, Supporting Information). Specifically, a significant fraction (≈21%) of the cells on fibronectin-coated crossbows with centrosomes in front of their nuclei, oriented toward the wide end, still started migrating in the opposite direction when released from confinement. Similarly, many (≈67%) cells with rear-facing centrosomes started migrating forward (Figure 5B). The apparent correlation between centrosome localization and cell displacement was slightly higher for cells released from mAb13, but ≈27–42% of these cells still migrated in a direction opposite to the initial front-rear orientation of their centrosome (Figure 5B). To investigate these unexpected findings in more detail, we plotted each centrosome orientation (in radians) against the future angular displacement of the same cell and compared the results to simulated data representing a true positive correlation. We did not observe any significant correlation between the initial centrosome orientation and the direction the cell started to migrate to after being released from fibronectin or mAb13, beyond the fact that both metrics were (independently) biased toward the wide end of the micropattern (Figure S8A–C, Supporting Information).

Despite the widely held notion that MTOC orientation is a key polarity cue that helps steer mesenchymal cell migration downstream of integrin-mediated signaling, membrane protrusion can also precede centrosome and Golgi reorientation during cell motility.[29,39,73] In such cases, centrosome reorientation toward the nascent lamellipodium is thought to stabilize polarized anterograde trafficking and cytoskeletal dynamics, promoting persistent migration. Acknowledging the higher front-rear polarity (centrosome orientation) and directional persistence of U-251MG cells released from fibronectin-coated micropatterns (Figure 4D; Figure S7D,E, Supporting Information), and the simultaneous lack of direct correlation between centrosome orientation and early migration (Figure S8A–C, Supporting Information), we sought to find out whether centrosome orientation correlated with directional persistence *after* the cells had been allowed to migrate freely. To this end, we plotted the average angle between current centrosome orientation (relative to the nucleus) and the corresponding cell movement vector and compared it to the final directionality ratio of the same cell. We observed a clear positive correlation between consistent centrosome orientation toward the leading edge and higher directional persistence (Figure 5C–E). Moreover, we observed several individual cells whose centrosomes were seemingly reorienting toward newly formed lamellipodia, preceding/during net cell movement in the same direction (Figure 5A). Together, these results suggest that centrosome orientation serves to stabilize protrusion and directional migration in U-251MG cells. This may also explain the higher overall directionality of cells leaving fibronectin-coated micropatterns, as centrosome orientation is more likely to coincide with the direction of migration when both metrics are already biased strongly (but independently) in the same direction. On the other hand, there was no consistent positive or negative correlation between centrosome orientation and overall cell speed (track length) across the analyzed samples (Figure S7F,G, Supporting Information). Thus, migration speed appears to be uncoupled from directionality when cells are released from spatial confinement, in contrast to the unrestricted migration of many different cell types,[72] although we cannot exclude astrocyte- or glioma-specific factors as a cause for these differences.

Our findings indicate that centrosome orientation alone is an incomplete proxy for front-rear polarity in migrating cells.

Figure 4. Biotinylation-based dynamic micropatterning enables the investigation of early spreading and migration events with high temporal resolution. A) Images depicting the migration of U-251MG cells from crossbow-shaped, FN- and mAb13-coated micropatterns to SA-FN-coated substrate. Color-coded (light orange to red) outlines indicate cell positions every 15 min, starting 10 min before the SA-FN was added, while the gray outlines depict the locations of the micropatterns. ROIs illustrate the locations of individual centrosomes (white arrows). Scale bars, 30 µm (main) and 10 µm (ROI). B) Rate of cell spreading after release from FN- and mAb13-coated micropatterns. Mean ± SD of $n = 27$ (mAb13)–31 (FN) cells, from three (FN) and four (mAb13) independent experiments. C) Tracks depicting the movement of individual cells from 10 min before to 60 min after their release on SA-FN, at 5 min intervals. The starting position (0,0) is indicated by a black cross. $n = 52$ (FN) and 52 (mAb13) cells, from three (FN) and four (mAb13) independent experiments. D) Angular histograms depicting centrosome orientation relative to the nucleus and micropattern in the cells 10 min before their release on SA-FN. $n = 52$ (FN) and 52 (mAb13) cells, from three (FN) and four (mAb13) independent experiments. E) Angular displacements of cells 60 min after their release on SA-FN, relative to their starting positions. $n = 52$ (FN) and 52 (mAb13) cells, from three (FN) and four (mAb13) independent experiments. F) Fluorescence images showing *F*-actin and its retrograde flow (kymographs) in cells confined on FN- and mAb13-coated micropatterns, and after release on SA-FN. Red boxes indicate regions presented over time in the corresponding kymographs, and dashed red lines highlight the slopes of moving actin features. Representative of two independent experiments. G) Quantification of actin flow rates in cells confined on FN- and mAb13-coated micropatterns, and after release on SA-FN. Values from $n = 7$ (FN)–13 (mAb13) cells, overlaid with sample means, from two independent experiments. Analyzed by ordinary one-way ANOVA and Sidak's multiple comparisons test.

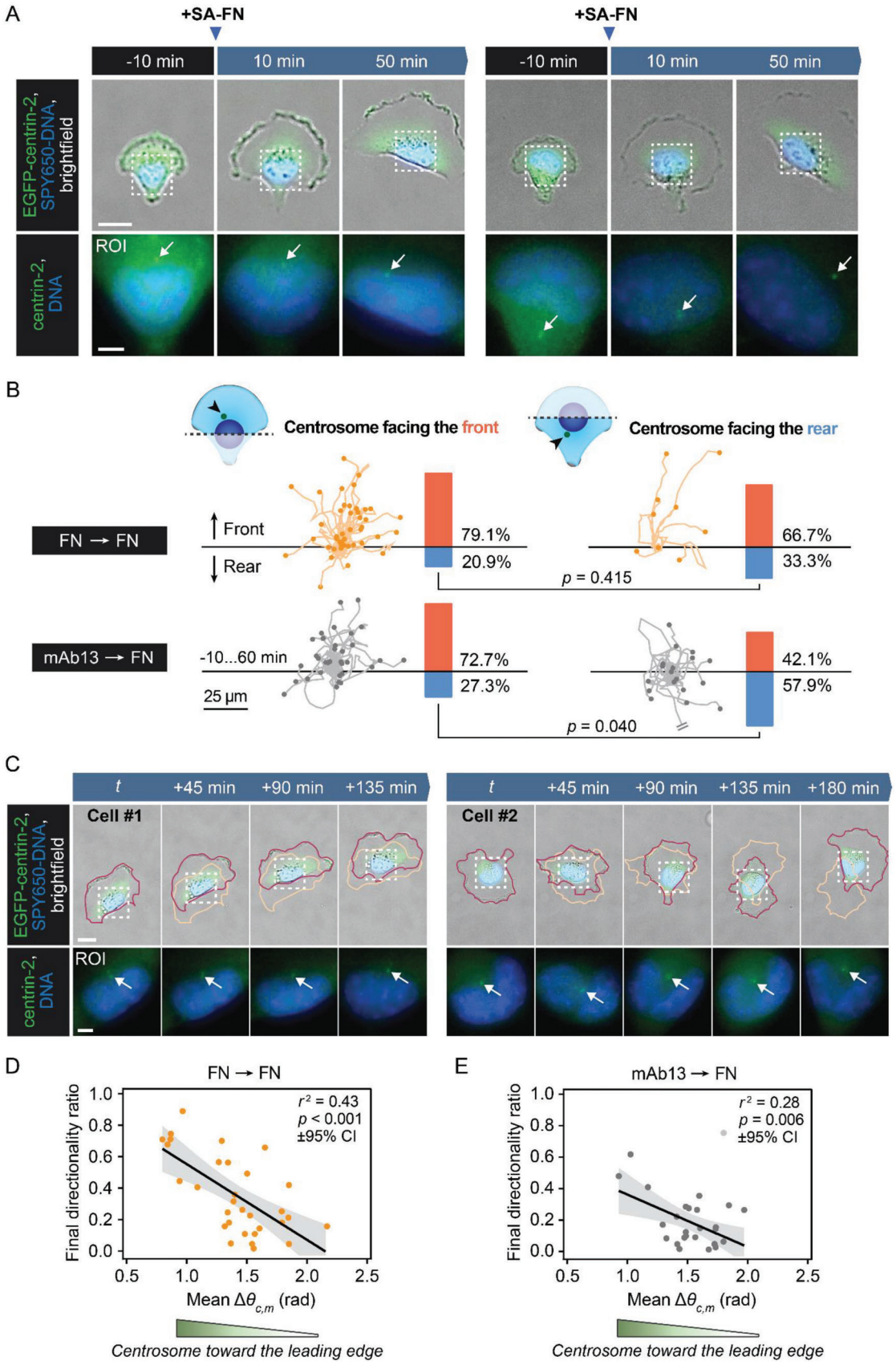

Indeed, a significant fraction of glioblastoma cells grown on anisotropic micropatterns failed to orient their centrosomes and nuclei in accordance with the rest of their polarized signaling and/or adhesive machinery, or this process was significantly delayed, leading to a comparatively poor correlation between centrosome orientation and early migration events. This is in line with a previously reported inability of the nucleus-Golgi axis to predict the direction of cell migration when cells are released from confinement without a predefined front-rear axis (i.e., without asymmetric substrate cues).[29,39] Here, multiple cells were observed to migrate toward the narrow end of the micropattern even when their own centrosomes were oriented in the opposite direction (Figure 5B). This indicates that even the MTOC orientation coupled with an asymmetric distribution of available integrin ligands is insufficient to fully dictate the direction of cell migration. Our results underscore the partially stochastic nature of single-cell migration, prompting an investigation of additional polarity markers and their dynamic regulation in micropattern-confined cells.

Some of the responses to the different ECM components reported here can likely be attributed to expression levels of various adhesive and cytoskeletal components, including the different integrin subunits. While other cell type-dependent effects are also possible, it is important to note that the prior studies suggesting a disconnect between MTOC polarization and cell migration were conducted using non-transformed stromal and epithelial cells.[29,39] This implies that the poor correlation between centrosome orientation and early migration may represent a more general feature of mammalian cells and would not be a cancer-related phenomenon.

Interestingly, micropatterned groups of kidney epithelial cells display strong collective Golgi polarization that is guided by substrate geometry.[25] This collective polarity requires intact cell–cell junctions and correlates with directed spreading when the cells are released from confinement. Cell–cell interactions are ubiquitous in most human tissues and have a profound impact on morphogenesis.[74] It is tempting to speculate that tissue-level organization of cells can reinforce responses to external geometric cues and, much like the collective durotaxis of epithelial monolayers,[75] robust directed migration appears as an emergent property.

3. Conclusion

Here, we describe a new method for dynamic micropatterning of cell culture substrates that represents an improvement over previously reported deep UV photopatterning techniques.[26,54] Based on commonly available commercial reagents, biotinylated PLL-g-PEG, and streptavidin-conjugated cell adhesion ligands, the new technique is compatible with different adhesion biochemistries, inexpensive, and easily adopted by individual research groups. In addition to being fully applicable to conventional static micropatterning with one or two different adhesive ligands, biotinylated PLL-g-PEG can be used for a rapid and controlled release of cells from spatial confinement. The micropatterned substrates are fully amenable to long-term cell culture, as well as high-resolution and live-cell imaging.

We employed biotinylation-based dynamic micropatterning to demonstrate that the well-recognized capacity of adherent cells to polarize and undergo directed migration in response to geometric cues[1,15,30] is directly influenced by the type of integrin ligand the cells are interacting with. Maximal front-rear polarity, i.e., centrosome orientation between the nucleus and leading edge, was achieved on anisotropic micropatterns coated with fibronectin or LN-521, whereas polarization was decreased on type I collagen. Integrin β1-clustering bivalent antibodies, 12G10 and mAb13, were also supportive of significant intracellular signaling responses and partial front-rear polarization without additional physiological integrin ligands. Curiously, the associated integrin conformation, active (12G10) versus inactive (mAb13), did not impact the degree of polarization. This suggests that planar polarity can be influenced by signaling downstream of integrin clustering alone, independent of receptor occupancy.[66] Together, these findings present interesting considerations for future studies on cell polarity and directed migration, especially in the context of more complex niche architectures and in vivo models where alternating and mixed matrix compositions are the norm.[76,77]

The cells released from fibronectin-coated micropatterns to fibronectin migrated with higher directional persistence than cells released from mAb13. However, we found that centrosome orientation, a commonly used readout for cell front-rear polarity in directed migration, only poorly predicted the direction of early cell spreading and migration from individual micropatterns—especially in cells moving from fibronectin to fibronectin. Instead, MTOC reorientation toward the leading edge may serve to stabilize polarized trafficking and protrusion, promoting persistent cell migration. Another commonly held notion states that cell spreading and migration are biased toward pre-existing lamellipodia and the cytoskeletal and signaling machinery within,[29,78] which explains the propensity of cells to polarize toward the more adhesive regions of anisotropic micropatterns.[15,28] Here, we observed that a number of glioblastoma cells were capable of ignoring both MTOC orientation and cellular shape cues, migrating "backward" from crossbow-shaped

Figure 5. Centrosome orientation alone does not dictate the direction of U-251MG migration, but may help stabilize it. A) Images of U-251MG cells before and after their release from FN-coated micropatterns on SA-FN. White arrows denote centrosomes, indicated by centrin-2. Scale bars, 20 µm (main) and 5 µm (ROI). B) Tracks of cells released from FN- and mAb13-coated micropatterns, stratified based on the initial centrosome orientation relative to the nucleus. One track pointing down has been shortened for clarity (indicated by two parallel lines). $n = 43$ (FN, centrosome in the front), 9 (FN, centrosome in the back), 33 (mAb13, centrosome in the front), and 19 (mAb13, centrosome in the back) cells, from three (FN) and four (mAb13) independent experiments. Analyzed by Fisher's exact test. C) Images of migrating U-251MG cells after their release from FN-coated micropatterns on SA-FN. White arrows denote centrosomes, indicated by fluorescent centrin-2. Colored outlines highlight current (dark red) and previous (light orange) cell positions. All time points are indicated relative to the first frame (t). Scale bars, 20 µm (main) and 5 µm (ROI). D) Scatterplot depicting the linear correlation between $\Delta\theta_{c,m}$ (mean difference between centrosome orientation relative to the nucleus and the corresponding cell movement vector) and final directionality ratio 4 h after the cells' release from FN-coated micropatterns. $n = 31$ cells, from three independent experiments. r^2, coefficient of determination. E) Scatterplot depicting the linear correlation between $\Delta\theta_{c,m}$ and final directionality ratio 4 h after the cells' release from mAb13-coated micropatterns. $n = 27$ cells, from four independent experiments. r^2, coefficient of determination. The data point depicted in light gray was excluded from the linear model (std. residual = 3.47).

micropatterns. This highlights the multifaceted nature of planar polarity in migrating cells, and calls into question some of the common proxies that are being used for studying it.

4. Experimental Section

Cell Lines and Transfections: U-251MG human glioblastoma cells were obtained from Dr. David J. Odde (University of Minnesota), authenticated using a short tandem repeat assay (Leibniz Institute DSMZ–German Collection of Microorganisms and Cell Cultures) and cultured in Dulbecco's modified Eagle's medium (DMEM)/F-12 (Gibco, 11320-074) with 8% fetal bovine serum (FBS) (Sigma, F7524). MDA-MB-231 human breast adenocarcinoma cells were purchased from the American type culture collection and authenticated using a short tandem repeat assay (DSMZ). U-2OS human osteosarcoma cells were acquired from DSMZ. MDA-MB-231 and U-2OS cells were cultured in high-glucose DMEM (Sigma, D5796-500ML) with 10% FBS (Sigma, F7524), 2 mM L-glutamine (Sigma, G7513-100ML) and 1x non-essential amino acids (Sigma, M7145-100ML). A20 mouse lymphoma cells stably expressing a hen egg lysozyme-specific IgM BCR (D1.3)[79] were obtained from Dr. Facundo Batista (The Ragon Institute of MGH, MIT, and Harvard) and cultured in RPMI 1640 with 2.05 mM L-glutamine, 10% FBS, 50 µM β-mercaptoethanol, 10 mM HEPES and 100 U mL^{-1} penicillin/streptomycin. All cell lines were tested for mycoplasma contamination and cultured at +37 °C/5% CO_2 in a humidified incubator.

U-251MG cells were transfected with pEGFP-centrin-2 (a gift from Dr. Erich Nigg, Addgene plasmid #41 147) using Lipofectamine 2000 (Thermo Fisher Scientific, 11 668 019). The cells were passaged onto a clean 6-well plate at ≈ 40% confluency and supplemented with 500 ng of the plasmid and 1.25 µL of the transfection reagent in 200 µL of Opti-MEM (Thermo Fisher Scientific, 31 985 070), for a final volume of 2 mL. The cells were incubated at +37 °C/5% CO_2 overnight. In order to produce a stable EGFP-centrin-2-expressing cell line, the transfected U-251MGs were selected over the course of 2 weeks by supplementing the growth medium with 400 µg mL^{-1} G418 (Sigma, G8168-10ML). Finally, the cells were sorted using Sony SH800 (Sony) to obtain a subpopulation with sufficiently high and even expression of the construct.

Antibodies and Reagents: The following primary antibodies were used in the study: ms anti-paxillin (BD Biosciences, 612 405), 1:200 for IF; rbt anti-paxillin (Abcam, ab32084), 1:250 for IF; ms anti-γ-tubulin (Abcam, ab11316), 1:250 for IF; rbt anti-TGN46 (Abcam, ab50595), 1:200 for IF; rat anti-centrin-2 (BioLegend, 698 602), 1:200 for IF; ms anti-FAK (BD Biosciences, 610 088), 1:1000 for WB; rbt anti-p-FAK (Y397) (Cell Signaling Technology, 8556), 1:100 for IF, 1:1000 for WB; ms anti-ERK1/2 (Cell Signaling Technology, 4696), 1:1000 for WB; rbt anti-p-ERK1/2 (T202/Y204) (Cell Signaling Technology, 4370), 1:1000 for WB; ms anti-AKT (Cell Signaling Technology, 2920), 1:1000 for WB; rbt anti-p-AKT (S473) (Cell Signaling Technology, 9271), 1:1000 for WB; rbt anti-fibronectin (Sigma, F3648), 1:150 for IF, 1:1000 for WB; ms anti-active integrin β1 (clone 12G10, in-house production), used as a substrate for cell adhesion at the indicated concentrations; rat anti-inactive integrin β1 (clone mAb13, in-house production), used as a substrate for cell adhesion at the indicated concentrations; goat anti-ms IgM Fab fragment (Jackson ImmunoResearch, 115-007-020), used as a substrate for B cell adhesion and activation at the indicated concentration.

The secondary antibodies used were Alexa Fluor 488/568/647-conjugated secondary antibodies raised against mouse (Invitrogen, A31571), 1:300 for IF; rabbit (Invitrogen, A21206, A11008, A10042 and A31573), 1:300 for IF; rat (Invitrogen, A21208 and A11077), 1:300 for IF; and goat (Invitrogen, A11055), 1:500 for IF; Azure Spectra 650 Ab goat anti-ms (Azure Biosystems, AC2166), 1:2500 for WB; Azure Spectra 800 Ab goat anti-rbt (Azure Biosystems, AC2134), 1:2500 for WB.

The following proteins and peptides were used as substrates for cell adhesion: fibronectin (PromoCell, C-43050), type I collagen (Sigma, C8919), recombinant human laminin 521 (BioLamina, LN521), collagen mimetic H-GPC(GPP)$_5$GFOGER(GPP)$_5$GPC-NH_2 (made to order by Auspep in Melbourne, Australia) and fibronectin fragment FNIII 7–10 (in-house production). FN-FITC (Sigma, F2733) was used to study secondary ligand binding to PLL-g-PEG-biotin. PF-573228 (MedChem, HY-10461) was used at 5 µM concentration for 90 min to inhibit FAK activity. Fluorescent bovine serum albumin (Thermo Fisher Scientific, A34786, A34785) and fibrinogen (Thermo Fisher Scientific, F35200) conjugates were used for visualizing micropatterns. The following fluorescent counterstains were used for visualizing DNA/nuclei and filamentous actin: DAPI (4′,6-diamidino-2-phenylindole), at 5 µg mL^{-1}; SPY555-DNA (Spirochrome, SC201, used for live cells) at 1:1000; SPY650-DNA (Spirochrome, SC501, used for live cells) at 1:1000; Alexa Fluor 488 phalloidin (Invitrogen, A12379) at 1:300; Acti-Stain 670 phalloidin (Cytoskeleton, PHDN1-A) at 1:300; and SPY650-Fastact (Spirochrome, SC505, used for live cells) at 1:1000.

Depletion of Fibronectin from Serum: Serum fibronectin was removed from FBS (Sigma, F7524) using liquid chromatography and 25 mL of Gelatin Sepharose 4B resin (Sigma, GE17-0956-01). Four plastic chromatography columns (Bio-Rad, 7 321 010) were each packed with 25% of the total resin (≈6 mL per column) and washed with ≥6 bed volumes of sterile PBS. Two of the columns were drained (excluding the bed), 500 mL of sterile FBS was split into two equally sized fractions on ice and these were run through the two columns. The eluates were collected in sterile glass bottles and kept on ice. Next, the eluates were pooled and the chromatography was repeated using the combined eluate and the two remaining columns. The resulting pooled eluate was sterile filtered using a 0.22 µm Stericup filter (Merck Millipore, SCGPU05RE) and stored at −20 °C.

The results of fibronectin depletion were confirmed by western blotting. Equal volumes of the original serum, first and second eluates, used resin from one of the first two columns, and a control sample comprising 100 µg mL^{-1} bovine plasma fibronectin (Sigma, 341631–5MG) in PBS were separated by SDS-PAGE and blotted with anti-fibronectin antibodies as described below.

Cell Adhesion to Coated Polystyrene Plates: For visualizing cell attachment and spreading on different ECM components and anti-integrin β1 antibodies at the indicated time points, polystyrene 96-well plates (Thermo Fisher Scientific, 08-772-53) were coated with 3,000 ng cm^{-2} of fibronectin, type I collagen, 12G10 or mAb13 for 2 h at +37 °C. These and untreated wells (negative control) were then blocked with 2% BSA/PBS for 15 min. U-251MG cells were allowed to adhere and spread in the different wells for 30 min before the samples were fixed with warm 4% PFA for 10 min, washed with PBS, and imaged.

In order to investigate the activation of signaling pathways upon cell spreading on the different substrates, polystyrene 6-well plates (Thermo Fisher Scientific, 08-772-49) were coated with fibronectin, type I collagen, 12G10 or mAb13 as described above. U-251MG cells were kept suspended in full medium for 30 min (+37 °C/5% CO_2), and then either incubated in suspension for an additional 30 min or allowed to spread on the coated 6-well plates for the same amount of time. Finally, the samples were collected and processed for immunoblotting as described below.

Western Blotting: Cells on multiwell plates were placed on ice, rinsed twice with ice-cold PBS, and scraped into lysis buffer comprising 50 mM Tris-HCl pH 7.5, 150 mM NaCl, 1% SDS, 0.5% Triton X-100, 5% glycerol, and protease (Roche, 0 505 648 9001) and phosphatase (Roche, 0 490 683 7001) inhibitors. Alternatively, cells in suspension were spun down and washed once with ice-cold PBS before lysis. The lysates were vortexed, placed on a heat block at +90 °C for 10 min, and sonicated before separation by SDS-PAGE on 4–20% Mini-PROTEAN TGX gels (Bio-Rad, 456–1096). The proteins were transferred to nitrocellulose membranes and visualized using a 1% Ponceau S staining solution. The membranes were blocked with AdvanBlock Fluor blocking buffer (Advansta, R-03729-E10) and incubated with the indicated primary antibodies overnight at +4 °C, followed by fluorophore-conjugated secondary antibodies for 1–2 h at room temperature (r.t.). The antibodies were diluted in AdvanBlock Fluor blocking buffer. Finally, the membranes were scanned using a Chemi-Doc MP imaging system (Bio-Rad).

Photopatterning of PLL-g-PEG-Coated Coverslips: UV photopatterning of non-biotinylated PLL-g-PEG surfaces has been described previously.[54] Here, glass coverslips were immersed in concentrated nitric acid for

5 min while being gently agitated, washed under running water for 3 min, and rinsed five times with deionized water and twice with abs. ethanol. The coverslips were air-dried and stored protected from dust. Before micropattern preparation, the acid-washed coverslips were exposed to deep UV light in the air (UVO-cleaner 342-220, Jelight Company; low-pressure mercury vapor lamp, fused quartz, λ = 185 and 254 nm, 30–33 mW cm^{-2} at 254 nm with the distance of ¼″) at 5 cm distance for 5 min. The coverslips were then coated by incubating them in 0.1 mg mL^{-1} PLL(20)-g[3.5]-PEG(2)/PEG(3.4)-biotin(50%) (SuSoS, Switzerland; for dynamic micropatterns) or PLL(20)-g[3.5]-PEG(2) (for static/conventional micropatterns) in 10 mM HEPES pH 7.4 for 1 h at r.t., washed twice with PBS and once with deionized water, air-dried and stored on the bench.

Quartz/chromium photomasks were obtained from Delta Mask (Netherlands). Each photomask was cleaned by two subsequent rinses with deionized water and ethanol, dried using airflow, and treated in the UVO-cleaner for 5 min before use. PLL-g-PEG-coated coverslips were inverted and placed on the photomask with drops of deionized water. The amount of water was adjusted to the coverslip size to allow a complete coverage of the interface, while still retaining the two surfaces in close proximity (e.g., ≈5 µL cm^{-2} of water was added and the excess was blotted away carefully using lint-free paper). The coverslips covered by the photomask were exposed to deep UV light for 6 min, carefully detached from the photomask by immersing them in deionized water, and air-dried. The resulting photopatterned coverslips can be stored on the bench or at +4 °C for several weeks. Before use, the micropatterns were coated with protein(s) as indicated below.

Preparation of Streptavidin-Conjugated Secondary Ligands: Streptavidin-conjugated proteins and peptides were prepared using commercial kits from Abnova (KA1556) and Abcam (ab102921) according to the manufacturers' instructions. Briefly, 1 µL of modifier reagent was added to each 10 µL of 1 mg mL^{-1} stock solution of the protein/peptide. The resulting solution was added onto the lyophilized material and incubated at r.t. for a minimum of 3 h. Afterward, 1 µL of quencher reagent was added to each 10 µL of the protein/peptide solution and the final conjugate was stored at +4 °C.

Measuring the Binding of Streptavidin-Conjugated Ligands to Biotinylated PLL-g-PEG: In order to measure the amount of SA-FN binding to the biotinylated PLL-g-PEG, coverslips with linear 9 µm wide micropatterns at 30 µm separation were prepared as described above. The coverslips were coated with 225 ng cm^{-2} fibronectin and 75 ng cm^{-2} BSA-AF555 in PBS for 1 h at r.t. by inverting each coverslip on a 20 µL droplet, placed on parafilm inside a foil-covered humidity chamber. The coverslips were washed twice with PBS and incubated with 0, 15, 75, or 225 ng cm^{-2} SA-FN in growth medium (DMEM/F-12) with 10% fibronectin-depleted FBS for 15 min at r.t. Next, the coverslips were washed once with medium and once with PBS, blocked for 10 min with 10% horse serum and prepared into IF samples (anti-fibronectin) as indicated below. After the samples had been imaged, data points corresponding to the immunofluorescence intensity of non-micropatterned regions of interest from different experiments were normalized using the area under the curve, and the relationship between SA-FN concentration and recorded immunofluorescence was investigated.

Binary Micropatterns with Different Primary and Secondary Ligands: Coverslips with linear 1.5 µm wide micropatterns at 5 µm separation, on PLL-g-PEG-biotin, were prepared as described above. The coverslips were coated with 1) 225 ng cm^{-2} type I collagen and 75 ng cm^{-2} BSA-AF555 or 2) 75 ng cm^{-2} BSA-AF555 only in PBS for 1 h at r.t., washed with PBS, and blocked by incubating them with 2% BSA/PBS for 30 min at r.t. The coated micropatterns were washed with PBS, incubated with 1) PBS or 2) 75 ng cm^{-2} SA-GFOGER for 15 min at r.t., and washed twice with PBS. The coverslips were seeded with MDA-MB-231 cells at ≈20% confluency. After 3 h at +37 °C/5% CO_2, the cells were fixed and prepared into immunofluorescence samples.

Stability of Streptavidin-Conjugated Ligands on Biotinylated PLL-g-PEG: Coverslips were cleaned and coated with biotinylated PLL-g-PEG as described above. Next, the coverslips were incubated with 225 ng cm^{-2} SA-FN for 15 min at r.t. to coat the PLL-g-PEG-biotin surface with the secondary ligand. The coverslips were washed with PBS, transferred onto clean 24-well plates, and immersed in a growth medium. Indicated wells were seeded with U-251MG cells at ≈2–15% confluency (for 6 days and 24 h time points, respectively) and the plates were maintained at +37 °C/5% CO_2 in a humidified incubator. After one to six days the samples were fixed and prepared for IF imaging as described below.

Kinetics of SA-FN Binding to Biotinylated PLL-g-PEG: In order to investigate the rate at which streptavidin-conjugated secondary ligands bind to the biotinylated PLL-g-PEG when cells were being released from confinement, coverslips with linear 9 µm wide micropatterns at 30 µm separation were prepared as described above. The coverslips were coated with 750 ng cm^{-2} fibronectin and 75 ng cm^{-2} BSA-AF555 for 1 h at r.t., and blocked by incubating them with 2% BSA/PBS for 10 min at r.t. The coated coverslips were immersed in a U-251MG growth medium, similar to the live-cell migration experiments described below. Using a confocal microscope, the distribution of SA-FN (FITC) in the focal plane next to the glass was recorded every 2 min, before and after supplementing the samples with 750 ng cm^{-2} SA-FN-FITC.

Seeding Cells on the Micropatterns: Before the photopatterned PLL-g-PEG(-biotin) coverslips were used for cell culture, the micropatterns were coated by incubating them with the indicated amounts and types of substrate molecules in PBS for 1 h at r.t. Next, the coverslips were washed with PBS, blocked with 2% BSA/PBS for 30 min at r.t., and washed twice more with PBS. The coverslips were either placed in 24-well plate wells (13 mm coverslips, for fixed samples) or assembled into imaging chambers using Attofluor components (Thermo Fisher Scientific, A7816; 25 mm coverslips, for live-cell imaging), and immersed in growth medium. Fibronectin-depleted serum was used in all experiments where substrates other than fibronectin were being used for coating the micropatterns. Cell suspension was prewarmed in the incubator for 5–10 min and cells were seeded on the micropatterned coverslips at ≈10% confluency. Unless otherwise noted, the cells were allowed to adhere and spread on the patterns for ≈ 3 h before they were fixed or used for experiments. Alternatively, an excess of cells was seeded on each coverslip and allowed to adhere for 10–20 min. The wells/imaging chambers were then tilted and washed carefully with a growth medium to get rid of the extra cells without allowing the micropatterned coverslip and cells to dry.

Comparing Cells and Micropatterns on Biotinylated Versus Non-Biotinylated PLL-g-PEG: U-251MG and U-2OS cells were confined on 37 µm wide crossbow-shaped micropatterns, on PLL-g-PEG and PLL-g-PEG-biotin, coated with 225 ng cm^{-2} fibronectin and 75 ng cm^{-2} fibrinogen (Fb)-AF647. After the cells had spread on the patterns, selected wells were supplemented with 375 ng cm^{-2} SA-FNIII 7–10 and the cells were allowed to move for 1 h before all the samples were fixed, processed into immunofluorescence samples, and imaged as described below. During subsequent analysis the images of individual patterns were reoriented, aligned, and average intensity projections were created from the actin and paxillin channels of confined cells (i.e., cells that were not supplemented with SA-FNIII 7–10) to investigate the mean distribution of these cytoskeletal and adhesion components in cells adhered to micropatterned PLL-g-PEG and PLL-g-PEG-biotin. Additionally, cell outlines were created by masking U-2OS cells using actin. The outlines were overlaid to study the role of PLL-g-PEG biotinylation in cell spreading on the extraneous SA-FNIII 7–10.

B Cell Activation Using Dynamic Micropatterns: A20 [D1.3] cells were adhered to round 5 µm wide micropatterns on PLL-g-PEG-biotin, coated with 150 ng cm^{-2} fibronectin and 37.5 ng cm^{-2} BSA-AF555. After the excess cells had been washed away, the remaining micropatterned cells were treated with 1100 ng cm^{-2} unconjugated or SA-anti-IgM Fab fragment for 10 min before fixation and processing into immunofluorescence samples as described below.

Live-Cell Migration Experiments Using Dynamic Micropatterns: U-251MG cells stably expressing EGFP-centrin-2 were confined on 37 µm wide crossbow-shaped micropatterns on PLL-g-PEG-biotin, coated with 750 ng cm^{-2} fibronectin or mAb13 and 75 ng cm^{-2} BSA-AF555/647. The nuclei were visualized using SPY555/650-DNA. After the cells had fully spread on the micropatterns, imaging (brightfield, centrin-2, and nuclei) was started and the cells were released to spread and migrate by adding 750 ng cm^{-2} SA-FN. Time points from 10 min before to 60 min after the

addition of SA-FN were imaged every 5 min, and subsequent time points were imaged every 15 min. To analyze the results, nuclei were segmented and tracked using a custom CellProfiler pipeline, while cell outlines and centrosomes were tracked using semiautomatic ImageJ scripts. Any potential time points after cells had collided with others to change their direction or had started undergoing apoptosis or mitosis were excluded from the analyses. The resulting data were compiled and analyzed using R to yield metrics about the cells' motility and front-rear polarization (i.e., centrosome orientation). See below for details about the software.

Measuring Actin Retrograde Flow: U-251MG cells were confined on 37 µm wide crossbow-shaped micropatterns on PLL-g-PEG-biotin, coated with 750 ng cm^{-2} fibronectin or mAb13 and 75 ng cm^{-2} BSA-AF555. Using a widefield microscope and SPY650-Fastact counterstain, the distribution of F-actin in the cells was recorded every 2 s, for 2 min at a time, with ≥5 min between each capture. After the first 2 min, the cells were released from the micropatterns using 750 ng cm^{-2} SA-FN. Light exposure was optimized and kept as low as possible to ensure cell viability over prolonged periods of imaging. After deep learning-assisted image enhancement (see below for details), triplicate kymographs were prepared from the leading edge(s) of each cell, at every time point. The average actin flow rate measured using the slopes of the features in the three kymographs was reported.

Immunofluorescence Sample Preparation: Samples were fixed with warm 4% PFA in the growth medium for 10 min, followed by permeabilization and blocking with 0.3% Triton X-100 in 10% horse serum (Gibco, 16050–122) for 20 min. Primary antibodies were diluted in 10% horse serum and samples were incubated with the antibody overnight at +4 °C. Secondary antibodies were diluted in PBS and samples were incubated with the antibody for 1–2 h at r.t. Where needed, actin and nuclei were visualized using different fluorescent counterstains as indicated above. Finally, the samples were mounted using Mowiol (Merck Millipore, 475 904) supplemented with 2.5% 1,4-diazabicyclo[2.2.2]octane (DABCO) (Sigma, D27802) and allowed to cure overnight at r.t. before imaging.

Light Microscopy: Fixed fluorescent specimens and SA-FN-FITC binding to PLL-g-PEG-biotin were imaged using a Marianas spinning disk confocal microscope with a Yokogawa CSU-W1 scanning unit, controlled by SlideBook 6 software (Intelligent Imaging Innovations). The objectives used were 20x/0.8 NA Plan-Apochromat (Zeiss), 40x/1.1 NA W LD C-Apochromat (Zeiss), 63x/1.4 NA O Plan-Apochromat (Zeiss) and 100x/1.4 NA O Plan-Apochromat (Zeiss). Images were acquired using an Orca Flash4 sCMOS camera (Hamamatsu Photonics). Example images depicting fluorescently labeled micropatterns were acquired using an EVOS fl microscope (Advanced Microscopy Group), 20x/0.45 NA PlanFluor objective (Advanced Microscopy Group) and ICX285AL CCD camera (Sony). The remaining samples were imaged using a Nikon Eclipse Ti2-E widefield microscope, controlled by NIS-Elements AR 5.11 software (Nikon). The objectives used were 20x/0.75 NA CFI Plan Apo Lambda (Nikon) and 40x/0.6 NA CFI S Plan Fluor ELWD ADM (Nikon). Images were acquired using an Orca Flash4 sCMOS camera (Hamamatsu Photonics). For live-cell imaging, the samples were maintained in a stage top humidified incubator (Okolab) at +37 °C/5% CO_2.

Image Analysis: Images were analyzed using ImageJ/Fiji v1.53t[80] and CellProfiler v4.2.4 (Broad Institute) software. For measuring cell front-rear polarization on anisotropic micropatterns, the images were rotated such that the wide adhesive ends of the crossbow-shaped patterns were pointing up. Centrosome orientation was then defined as the angle of the vector connecting the centroid of the cell's nucleus to the centrosome.

For visualizing SA-FN accumulation on biotinylated PLL-g-PEG, immunofluorescence intensity profiles over linear regions of ≈ 160 µm were recorded. The profiles were smoothed by taking a moving average with a window size of 5 pixels.

Fluorescence microscopy data depicting actin flow in U-251MG cells were enhanced using the deep learning algorithm content-aware image restoration[81] implemented in the ZeroCostDL4Mic platform.[82] The custom model was trained from scratch for 100 epochs on 500 paired image patches [image dimensions: (2044, 2048), patch size: (400400)] with a batch size of 16 and a laplace loss function, using the CARE 2D ZeroCostDL4Mic notebook (v1). Key python packages used include tensorflow (v0.1.12), Keras (v2.3.1), csbdeep (v0.7.2), numpy (v1.21.6), and cuda (v11.1.105Build cuda_11.1.TC455_06.29190527_0). The training was accelerated using a Tesla T4 GPU.

Statistical Analysis: Statistical analyses and plotting were performed using Prism v6.07 (GraphPad Software) and R v4.2.2 (R Core Team) running on RStudio v.2022.07.2 (Rstudio Team). The following R packages were also used: circular,[83] BAMBI,[84] and ggplot2.[85] Circular correlation between two paired angles was measured using the R function cor.circular. For simulating paired circular data with a true positive correlation, a sample was drawn from a bivariate von Mises distribution using the function rvmsin with the following arguments: $n = 50$, kappa1 = 0.8, kappa2 = 0.8, kappa3 = 1, mu1 = 0, mu2 = 0. The sample was visualized and analyzed for circular correlation as described above.

Whenever data were deemed to follow a non-normal distribution (according to Shapiro-Wilk normality test), hypothesis testing was conducted using non-parametric methods. For linear regression analyses, data with standardized residuals >3 were considered outliers. Two-sided *p*-values were reported, and *p*-values <0.05 were considered statistically significant. The names and/or numbers of individual statistical tests, samples, and data points were indicated in figure legends.

Supporting Information

Supporting Information is available from the Wiley Online Library or from the author.

Acknowledgements

The authors thank Petra Laasola and Jenni Siivonen for their expert technical assistance, Guillaume Jacquemet for help with microscopy, and the Ivaska Lab members for insightful feedback and discussion. The Cell Imaging and Cytometry Core facility (Turku Bioscience, University of Turku, Åbo Akademi University, and Biocenter Finland), and Turku Bioimaging are acknowledged for services, instrumentation, and expertise. This work was supported by the Finnish Cancer Institute (K. Albin Johansson Professorship to J.I.); Research Council of Finland research projects (grant no. 325464 to J.I.; 25700, 296684 and 307313 to P.K.M.) and Centre of Excellence program (grant no. 346131 to J.I.); the Cancer Foundation Finland (to J.I.); the Sigrid Jusélius Foundation (to J.I. and P.K.M.); the Jane and Aatos Erkko Foundation (to J.I.); the Research Council of Finland InFLAMES Flagship Programme (grant no. 337530); University of Turku Doctoral Programme in Molecular Life Sciences (to A.I.) and Molecular Medicine (to S.H-P.); the Finnish Cultural Foundation (to A.I. and S.H-P.); the Orion Research Foundation (to A.I.); and the K. Albin Johansson's Foundation (to A.I.).

Conflict of Interest

The authors declare no conflict of interest.

Author Contributions

A.I., J.A., and J.I. performed conceptualization. A.I., J.A., S.H-P., and K.S. performed data curation. A.I., J.A., and K.S. performed formal analysis. P.K.M. and J.I. acquired funding. A.I., J.A., S.H-P., K.S., and M.S. performed investigation. A.I., J.A., and S.H.-P. performed methodology. P.K.M. and J.I. performed project administration. P.K.M. and J.I. acquired resources. A.I. and K.S. acquired software. P.K.M. and J.I. performed supervision. A.I., J.A., S.H-P., K.S., and M.S. performed validation. A.I., J.A., and K.S. performed visualization. A.I. and J.I. wrote the original draft. All authors reviewed and edited the manuscript.

Data Availability Statement

The data that support the findings of this study are available from the corresponding author upon reasonable request.

Keywords

cell migration, cell polarity, extracellular matrices, micropatterns

Received: June 8, 2023
Revised: October 3, 2023
Published online: November 5, 2023

[1] M. Théry, V. Racine, M. Piel, A. Pépin, A. Dimitrov, Y. Chen, J.-B. Sibarita, M. Bornens, *Proc. Natl. Acad. Sci. U. S. A.* **2006**, *103*, 19771.
[2] S. Huda, S. Soh, D. Pilans, M. Byrska-Bishop, J. Kim, G. Wilk, G. G. Borisy, K. Kandere-Grzybowska, B. A. Grzybowski, *J. Cell Sci.* **2012**, *125*, 5790.
[3] P. J. Albert, U. S. Schwarz, *Cell Adhes. Migr.* **2016**, *10*, 516.
[4] C. S. Chen, M. Mrksich, S. Huang, G. M. Whitesides, D. E. Ingber, *Science* **1997**, *276*, 1425.
[5] M. Burute, M. Prioux, G. Blin, S. Truchet, G. Letort, Q. Tseng, T. Bessy, S. Lowell, J. Young, O. Filhol, M. Théry, *Dev. Cell* **2017**, *40*, 168.
[6] T. Haremaki, J. J. Metzger, T. Rito, M. Z. Ozair, F. Etoc, A. H. Brivanlou, *Nat. Biotechnol.* **2019**, *37*, 1198.
[7] M. Théry, *J. Cell Sci.* **2010**, *123*, 4201.
[8] J.-I. Edahiro, K. Sumaru, Y. Tada, K. Ohi, T. Takagi, M. Kameda, T. Shinbo, T. Kanamori, Y. Yoshimi, *Biomacromolecules* **2005**, *6*, 970.
[9] J. Nakanishi, Y. Kikuchi, T. Takarada, H. Nakayama, K. Yamaguchi, M. Maeda, *Anal. Chim. Acta* **2006**, *578*, 100.
[10] C. G. Rolli, H. Nakayama, K. Yamaguchi, J. P. Spatz, R. Kemkemer, J. Nakanishi, *Biomaterials* **2012**, *33*, 2409.
[11] T. Vignaud, R. Galland, Q. Tseng, L. Blanchoin, J. Colombelli, M. Théry, *J. Cell Sci.* **2012**, *125*, 2134.
[12] M. J. Salierno, A. J. García, A. Del Campo, *Adv. Funct. Mater.* **2013**, *23*, 5974.
[13] W.-S. Yeo, M. N. Yousaf, M. Mrksich, *J. Am. Chem. Soc.* **2003**, *125*, 14994.
[14] X. Jiang, R. Ferrigno, M. Mrksich, G. M. Whitesides, *J. Am. Chem. Soc.* **2003**, *125*, 2366.
[15] X. Jiang, D. A. Bruzewicz, A. P. Wong, M. Piel, G. M. Whitesides, *Proc. Natl. Acad. Sci. U. S. A.* **2005**, *102*, 975.
[16] S. Raghavan, R. A. Desai, Y. Kwon, M. Mrksich, C. S. Chen, *Langmuir* **2010**, *26*, 17733.
[17] M. Hirose, M. Yamato, O. H. Kwon, M. Harimoto, A.i Kushida, T. Shimizu, A. Kikuchi, T. Okano, *Yonsei Med. J.* **2000**, *41*, 803.
[18] Y. Tsuda, A. Kikuchi, M. Yamato, A. Nakao, Y. Sakurai, M. Umezu, T. Okano, *Biomaterials* **2005**, *26*, 1885.
[19] K.-I. Nakajima, K. Zhu, Y.-H. Sun, B. Hegyi, Q. Zeng, C. J. Murphy, J. V. Small, Y. Chen-Izu, Y. Izumiya, J. M. Penninger, M. Zhao, *Nat. Commun.* **2015**, *6*, 8532.
[20] R. A. Alghamdi, M. Exposito-Rodriguez, P. M. Mullineaux, G. N. Brooke, P. P. Laissue, *Front. Cell Dev. Biol.* **2021**, *9*, 738786.
[21] P.-O. Strale, A. Azioune, G. Bugnicourt, Y. Lecomte, M. Chahid, V. Studer, *Adv. Mater.* **2016**, *28*, 2024.
[22] N. M. Rodriguez, R. A. Desai, B. Trappmann, B. M. Baker, C. S. Chen, *Langmuir* **2014**, *30*, 1327.
[23] A. Perl, D. N. Reinhoudt, J. Huskens, *Adv. Mater.* **2009**, *21*, 2257.
[24] P. Costa, J. E. Gautrot, J. T. Connelly, *Acta Biomater.* **2014**, *10*, 2415.
[25] P. Costa, L. M. Blowes, A. C. Laly, J. T. Connelly, *Acta Biomater.* **2021**, *126*, 291.
[26] S. F. M. Van Dongen, P. Maiuri, E. Marie, C. Tribet, M. Piel, *Adv. Mater.* **2013**, *25*, 1687.
[27] G. Mahmud, C. J. Campbell, K. J. M. Bishop, Y. A. Komarova, O. Chaga, S. Soh, S. Huda, K. Kandere-Grzybowska, B. A. Grzybowski, *Nat. Phys.* **2009**, *5*, 606.
[28] G. Kumar, C. C. Co, C.-C. Ho, *Langmuir* **2011**, *27*, 3803.
[29] B. Chen, G. Kumar, C. C. Co, C.-C. Ho, *Sci. Rep.* **2013**, *3*, 2827.
[30] G. Lee, S.-B. Han, D.-H. Kim, *Biomaterials* **2021**, *268*, 120548.
[31] S. Etienne-Manneville, *Oncogene* **2008**, *27*, 6970.
[32] C. D. Lawson, A. J. Ridley, *J. Cell Biol.* **2017**, *217*, 447.
[33] E. R. Gomes, S. Jani, G. G. Gundersen, *Cell* **2005**, *121*, 451.
[34] N. Osmani, F. Peglion, P. Chavrier, S. Etienne-Manneville, *J. Cell Biol.* **2010**, *191*, 1261.
[35] S. Seetharaman, S. Etienne-Manneville, *Trends Cell Biol.* **2020**, *30*, 720.
[36] A. I. Gotlieb, L. M. May, L. Subrahmanyan, V. I. Kalnins, *J. Cell Biol.* **1981**, *91*, 589.
[37] A. Kupfer, D. Louvard, S. J. Singer, *Proc. Natl. Acad. Sci. U. S. A.* **1982**, *79*, 2603.
[38] M. Martin, A. Veloso, J. Wu, E. A. Katrukha, A. Akhmanova, *Elife* **2018**, *7*, e33864.
[39] K. Vaidziulyte, A.-S. Macé, A. Battistella, W. Beng, K. Schauer, M. Coppey, *Elife* **2022**, *11*, e69229.
[40] N. M. Wakida, E. L. Botvinick, J. Lin, M. W. Berns, *PLoS One* **2010**, *5*, e15462.
[41] S. J. Stehbens, M. Paszek, H. Pemble, A. Ettinger, S. Gierke, T. Wittmann, *Nat. Cell Biol.* **2014**, *16*, 558.
[42] B. Bance, S. Seetharaman, C. Leduc, B. Boëda, S. Etienne-Manneville, *J. Cell Sci.* **2019**, *132*, jcs225805.
[43] S. Seetharaman, B. Vianay, V. Roca, A. J. Farrugia, C. De Pascalis, B. Boëda, F. Dingli, D. Loew, S. Vassilopoulos, A. Bershadsky, M. Théry, S. Etienne-Manneville, *Nat. Mater.* **2022**, *21*, 366.
[44] K. Vaidziulyte, A.-S. Macé, A. Battistella, W. Beng, K. Schauer, M. Coppey, *Elife* **2022**, *11*, e69229.
[45] J. C. M. Meiring, B. I. Shneyer, A. Akhmanova, *Curr. Opin. Cell Biol.* **2020**, *62*, 86.
[46] M. Maninová, Z. Klímová, J. T. Parsons, M. J. Weber, M. P. Iwanicki, T. Vomastek, *J. Mol. Biol.* **2013**, *425*, 2039.
[47] F. Dubois, K. Alpha, C. E. Turner, *Mol. Biol. Cell* **2017**, *28*, 3815.
[48] M. R. Chastney, J. R. W. Conway, J. Ivaska, *Curr. Biol.* **2021**, *31*, R536.
[49] S. Etienne-Manneville, A. Hall, *Cell* **2001**, *106*, 489.
[50] E. A. Cox, S. K. Sastry, A. Huttenlocher, *Mol. Biol. Cell* **2001**, *12*, 265.
[51] G. Klein, M. Langegger, R. Timpl, P. Ekblom, *Cell* **1988**, *55*, 331.
[52] W. Yu, A. Datta, P. Leroy, L. E. O'brien, G. Mak, T.-S. Jou, K. S. Matlin, K. E. Mostov, M. M. P. Zegers, *Mol. Biol. Cell* **2005**, *16*, 433.
[53] M. L. Kutys, K. M. Yamada, *Nat. Cell Biol.* **2014**, *16*, 909.
[54] A. Azioune, M. Storch, M. Bornens, M. Théry, M. Piel, *Lab Chip* **2009**, *9*, 1640.
[55] N. M. Green, *Methods Enzymol.* **1990**, *184*, 51.
[56] Y. Jiu, J. Lehtimäki, S. Tojkander, F. Cheng, H. Jäälinoja, X. Liu, M. Varjosalo, J. E. Eriksson, P. Lappalainen, *Cell Rep.* **2015**, *11*, 1511.
[57] A. Isomursu, K.-Y. Park, J. Hou, B. Cheng, M. Mathieu, G. A. Shamsan, B. Fuller, J. Kasim, M. M. Mahmoodi, T. J. Lu, G. M. Genin, F. Xu, M. Lin, M. D. Distefano, J. Ivaska, D. J. Odde, *Nat. Mater.* **2022**, *21*, 1081.
[58] E. Kuokkanen, V. Sustar, P. K. Mattila, *Traffic* **2015**, *16*, 311.
[59] C. Liu, H. Miller, K. L. Hui, B. Grooman, S. Bolland, A. Upadhyaya, W. Song, *J. Immunol.* **2011**, *187*, 230.
[60] C. Volkmann, N. Brings, M. Becker, E. Hobeika, J. Yang, M. Reth, *EMBO J.* **2016**, *35*, 2371.
[61] J. C. Wang, Y.-I.n Yim, X. Wu, V. Jaumouille, A. Cameron, C. M. Waterman, J. H. Kehrl, J. A. Hammer, *Elife* **2022**, *11*, e72805.
[62] S. Hu, T.-H. Chen, Y. Zhao, Z. Wang, R. H. W. Lam, *Langmuir* **2018**, *34*, 1750.
[63] A. Sarkar, D. N. Levine, N. Kuzmina, Y. Zhao, X. Wang, *Curr. Biol.* **2020**, *30*, 4022.
[64] R. Nishiuchi, J. Takagi, M. Hayashi, H. Ido, Y. Yagi, N. Sanzen, T. Tsuji, M. Yamada, K. Sekiguchi, *Matrix Biol.* **2006**, *25*, 189.
[65] L. Yap, H. G. Tay, M. T. X. Nguyen, M. S. Tjin, K. Tryggvason, *Trends Cell Biol.* **2019**, *29*, 987.
[66] S. Miyamoto, S. K. Akiyama, K. M. Yamada, *Science* **1995**, *267*, 883.

[67] G. Mana, D. Valdembri, J. A. Askari, Z. Li, P. Caswell, C. Zhu, M. J. Humphries, C. Ballestrem, G. Serini, *Life Sci Alliance* **2023**, *6*, e202201388.
[68] M. Fructuoso, M. Legrand, A. Mousson, T. Steffan, R. Vauchelles, J. De Mey, E. Sick, P. Rondé, D. Dujardin, *Biol Cell* **2020**, *112*, 53.
[69] P. A. Dimilla, K. Barbee, D. A. Lauffenburger, *Biophys. J.* **1991**, *60*, 15.
[70] C. E. Chan, D. J. Odde, *Science* **2008**, *322*, 1687.
[71] L. B. Case, C. M. Waterman, *Nat. Cell Biol.* **2015**, *17*, 955.
[72] P. Maiuri, J.-F. Rupprecht, S. Wieser, V. Ruprecht, O. Bénichou, N. Carpi, M. Coppey, S. De Beco, N. Gov, C.-P. Heisenberg, C. Lage Crespo, F. Lautenschlaeger, M. Le Berre, A.-M. Lennon-Dumenil, M. Raab, H.-R. Thiam, M. Piel, M. Sixt, R. Voituriez, *Cell* **2015**, *161*, 374.
[73] M. Ueda, R. Gräf, H. K. Macwilliams, M. Schliwa, U. Euteneuer, *Proc. Natl. Acad. Sci. U. S. A.* **1997**, *94*, 9674.
[74] H. A. Le, R. Mayor, *Biochem. Soc. Trans.* **2023**, *51*, 1733.
[75] R. Sunyer, V. Conte, J. Escribano, A. Elosegui-Artola, A. Labernadie, L. Valon, D. Navajas, J. M. García-Aznar, J. J. Muñoz, P. Roca-Cusachs, X. Trepat, *Science* **2016**, *353*, 1157.
[76] A. E. Mayorca-Guiliani, C. D. Madsen, T. R. Cox, E. R. Horton, F. A. Venning, J. T. Erler, *Nat. Med.* **2017**, *23*, 890.
[77] A. Isomursu, M. Lerche, M. E. Taskinen, J. Ivaska, E. Peuhu, *Exp. Cell Res.* **2019**, *378*, 217.
[78] A. Brock, E. Chang, C.-C. Ho, P. Leduc, X. Jiang, G. M. Whitesides, D. E. Ingber, *Langmuir* **2003**, *19*, 1611.
[79] G. T. Williams, C. J. Peaker, K. J. Patel, M. S. Neuberger, *Proc. Natl. Acad. Sci. U. S. A.* **1994**, *91*, 474.
[80] J. Schindelin, I. Arganda-Carreras, E. Frise, V. Kaynig, M. Longair, T. Pietzsch, S. Preibisch, C. Rueden, S. Saalfeld, B. Schmid, J.-Y. Tinevez, D. J. White, V. Hartenstein, K. Eliceiri, P. Tomancak, A. Cardona, *Nat. Methods* **2012**, *9*, 676.
[81] M. Weigert, U. Schmidt, T. Boothe, A. Müller, A. Dibrov, A. Jain, B. Wilhelm, D. Schmidt, C. Broaddus, S. Culley, M. Rocha-Martins, F. Segovia-Miranda, C. Norden, R. Henriques, M. Zerial, M. Solimena, J. Rink, P. Tomancak, L. Royer, F. Jug, E. W. Myers, *Nat. Methods* **2018**, *15*, 1090.
[82] L. Von Chamier, R. F. Laine, J. Jukkala, C. Spahn, D. Krentzel, E. Nehme, M. Lerche, S. Hernández-Pérez, P. K. Mattila, E. Karinou, S. Holden, A. C. Solak, A. Krull, T.-O. Buchholz, M. L. Jones, L. A. Royer, C. Leterrier, Y. Shechtman, F. Jug, M. Heilemann, G. Jacquemet, R. Henriques, *Nat. Commun.* **2021**, *12*, 2276.
[83] U. Lund, C. Agostinelli, H. Arai, A. Gagliardi, E. García-Portugués, D. Giunchi, J.-O. Irisson, M. Pocernich, F. Rotolo, https://CRAN.R-project.org/package=circular (accessed: December **2022**).
[84] S. Chakraborty, S. W. K. Wong, https://CRAN.R-project.org/package=BAMBI (accessed: December **2022**).
[85] H. Wickham, W. Chang, L. Henry, T. L. Pedersen, K. Takahashi, C. Wilke, K. Woo, H. Yutani, D. Dunnington, https://CRAN.R-project.org/package=ggplot2 (accessed: December **2022**).

